78 J. Med. Chem. 2011, 54, 78–94
DOI: 10.1021/jm100679e

Journal of Medicinal Chemistry Article

Integration of Lead Optimization with Crystallography for a Membrane-Bound Ion Channel Target: Discovery of a New Class of AMPA Receptor Positive Allosteric Modulators†

Simon E. Ward,*,‡ Mark Harries,§ Laura Aldegheri,∥ Nigel E. Austin,§ Stuart Ballantine,∞ Elisa Ballini,∥ Daniel M. Bradley,§ Benjamin D. Bax,∞ Brian P. Clarke,∞ Andrew J. Harris,§ Stephen A. Harrison,# Rosemary A. Melarange,§ Claudette Mookherjee,§ Julie Mosley,∞ Gianni Dal Negro,⊥ Beatrice Oliosi,∥ Kathrine J. Smith,∞ Kevin M. Thewlis,§ Patrick M. Woollard,§ and Shahnaz P. Yusaf∞

‡School of Life Sciences, University of Sussex, Brighton, BN1 9QJ, United Kingdom, §Neurosciences Centre of Excellence for Drug Discovery, GlaxoSmithKline, New Frontiers Science Park, Third Avenue, Harlow, Essex, CM19 5AW, United Kingdom, ∥Molecular Discovery Research, ⊥Laboratory Animal Science Worldwide, Medicines Research Centre, GlaxoSmithKline, Via A. Fleming, 4, 37100, Verona, Italy, #Respiratory Centre of Excellence for Drug Discovery, and ∞Molecular Discovery Research, Medicines Research Centre, GlaxoSmithKline, Gunnels Wood Road, Stevenage, SG1 2NY, United Kingdom

Received June 6, 2010

A novel series of AMPAR positive modulators is described that were identified by high throughput screening. The molecules of the series have been optimized from a high quality starting point hit to afford excellent developability, tolerability, and efficacy profiles, leading to identification of a clinical candidate. Unusually for an ion channel target, this optimization was integrated with regular generation of ligand-bound crystal structures and uncovered a novel chemotype with a unique and highly conserved mode of interaction via a trifluoromethyl group.

Introduction

Abnormalities in glutamatergic signaling are presumed to underlie a number of debilitating psychiatric diseases.[1] As such, interventions to modulate this signaling pathway offer considerable promise as approaches to design new medicines to treat a range of conditions including schizophrenia, depression, and cognitive impairment. α-Amino-3-hydroxyl-5-methyl-4-isoxazole propionate receptors (AMPAR[a]) mediate the majority of fast excitatory signaling in the central nervous system (CNS)[2] and consequently represent an appealing target; however, molecules able to act directly on AMPARs as either partial or full agonists could lead to uncontrolled central stimulation and so, inevitably, be poorly tolerated. Unsurprisingly, as a consequence of this, positive modulation of the AMPAR has been an attractive approach to mitigate this risk, allowing both spatial and temporal control of potentiation of AMPAR-mediated currents and so improving tolerability. In essence, AMPAR positive modulators have no effect upon channel currents per se and are only able to enhance ion flux through the receptor in the presence of the endogenous ligand glutamate. These modulators have been extensively characterized in vitro and in vivo, in particular linking potentiation of AMPAR to enhancement of cognitive function a key process required for learning and memory.[3,4] However, despite this considerable body of preclinical data, there still remains a lack of convincing late stage clinical data and no molecules have yet to progress to large scale phase III evaluation.[5]

A component of this failure is potentially contained in the lack of chemical diversity that has been explored. There are a sizable number of patents and papers describing new chemical entities, but all can be grouped into three main chemotypes based on those that have been progressed clinically (see reviews and references therein).[6,7] In brief, clinically evaluated molecules fall into the benzamide class exemplified by **1** (CX-691, Cortex), the benzothiadiazines class exemplified by **2** (S-18986, Servier), and the phenethylsulfonamide class exemplified by **3** (LY450108, Lilly). Most recently, we have described the discovery, characterization, and preliminary human PK data for our clinical candidate **4** (Figure 1).[8]

In tandem with this clinical investigation, considerable progress has also been made in understanding the structure of the AMPAR, which is a tetrameric structure comprising four subunits (GluA1−4) and which exhibits considerable heterogeneity of composition. In addition to the various subunit permutations, an additional layer of complexity is created by the existence of a number of splice variants and sites for post-translational modification. The gross structure of the receptor covers a large extracellular N-terminal domain that is

†The structures of the complexes of the five compounds **7a**, **7l**, **9a**, **10a**, and **19b** have been deposited with the Protein Data Bank (http://www.pdb.org/pdb/home/home.do) with the following accession codes: complex with **7a**, 2xx8; complex with **7l**, 2xx9; complex with **9a**, 2xx7; complex with **10a**, 2xxh; complex with **19b**, 2xxi.

*To whom correspondence should be addressed. Phone: +44 (0)1273 678359. Fax: +44 (0) 1273 876687. E-mail: simon.ward@sussex.ac.uk.

[a] Abbreviations: AMPA, α-amino-3-hydroxyl-5-methyl-4-isoxazole propionate; AMPAR, α-amino-3-hydroxyl-5-methyl-4-isoxazole propionate receptor; AUC, area under the curve; CDI, 1,1′-carbonyldiimidazole; BTB, brain tissue binding; CNS, central nervous system; DMSO, dimethylsulfoxide; FLIPR, fluorescence imaging plate reader; HATU, (2-(7-aza-1*H*-benzotriazole-1-yl)-1,1,3,3-tetramethyluronium hexafluorophosphate); LBD, ligand-binding domain; LTP, long-term potentiation; MED, minimally effective dose; MEST, maximal electroshock threshold test; NMDA, *N*-methyl-D-aspartic acid; NOR, novel object recognition; NSF, *N*-ethylmaleimide-sensitive fusion protein; PDZ, postsynaptic density protein 95; PPB, plasma protein binding; PSA, polar surface area; TARP, transmembrane α-amino-3-hydroxyl-5-methyl-4-isoxazole propionate regulatory protein; THF, tetrahydrofuran.

 Published on Web 12/03/2010

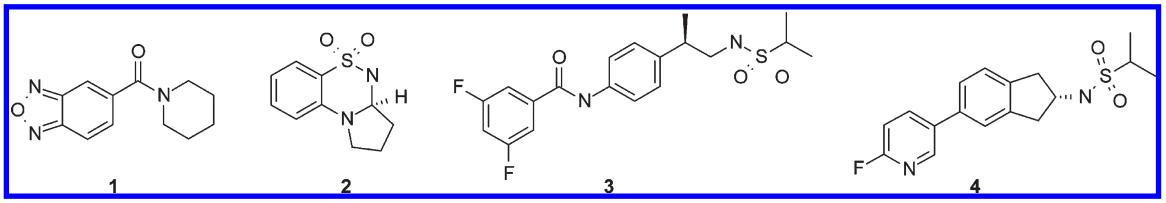

Figure 1. Example AMPAR positive modulators that have been progressed to clinical trials.

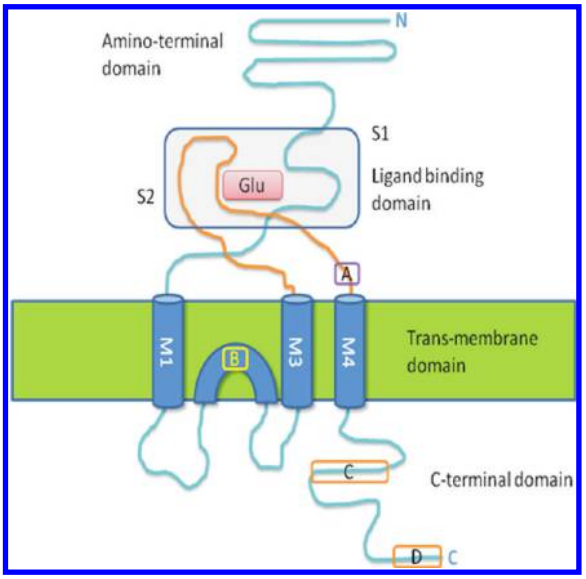

Figure 2. Schematic of single subunit of AMPAR key domains, LBD with S1 and S2 polypeptides colored differently. Key residue regions are highlighted: A, flip/flop splice variants; B, post-translational modification sites regulating Ca^{2+} permeability; C, NSF binding domain; D, PDZ binding domain.

responsible for the assembly of subunits, a LBD including the two polypeptide segments S1 and S2, a transmembrane region made up of three transmembrane domains (M1, M3, and M4), and a re-entrant loop (M2) and a C-terminal intracellular domain containing binding site motifs for a number of regulatory and trafficking proteins (Figure 2). While the latest structural data have come from the recent important publication of the crystallization and structural elucidation of the rat GluA2 receptor at 3.6 Å in complex with a competitive antagonist,[9] earlier studies focused on the S1S2 hybrid proteins. These crystal structures have shown positive allosteric modulators binding at the LBD dimer interface between two subunits, and simplistically they are thought to slow deactivation by stabilizing the clamshell dimer in its closed cleft glutamate bound conformation and/or slow desensitization by stabilizing the dimer interface.[9−12]

Following our previous work in this area, the objective of our current program of research was to identify novel chemotypes to progress differentiated AMPAR modulators into clinical studies. To achieve this goal, we embarked on a high throughput screen and sought to generate our own ligand-bound X-ray crystal structures to expedite the hit identification and optimization process. This article describes the development of one of the hits from this screen into a novel chemical series and its subsequent optimization to identify a clinical development candidate.

Chemistry

From our high throughput screen output, we selected **7a** as an attractive hit molecule, from which we prepared a number of initial analogues for which we maintained the tetrahydroindazole and phenyl rings as a constant, and varied the substituent on the phenyl ring (Scheme 1). The key transformation used for preparation of these molecules was the copper(I) mediated, microwave-assisted Ullmann-type coupling reaction, which proved to be superior in terms of yield and generality over other coupling methods investigated. Consequently, target molecules **7a**−**r** were prepared from 3-(trifluoromethyl)-4,5,6,7-tetrahydro-1*H*-indazole **5** by heating in the presence of a copper(I) source, chelating amine such as *trans*-1,2-diaminocyclohexane or *N*,*N*-dimethylglycine and base with an appropriate coupling partner **6a**−**r**. These coupling reactions worked well with either the iodine or bromine on **6** as outlined in Scheme 1. The various coupling partners **6a**−**r** used were either available commercially or prepared via standard amide formation and halogenation methods as detailed in the Experimental Section.

For amide analogues **9a**−**d** and **10a**,**b**, the benzoic acid ester **7o** or the phenylacetic acid ester **7p** was saponified to generate the respective carboxylic acids **8a** and **8b**, before being subjected to standard amide coupling conditions to afford benzamide derivatives **9a**−**d** and phenylacetamide derivatives **10a**,**b**. The homologated pyrrolidine amide **10a** was also reacted further with the electrophilic fluorinating agent 2-fluoro-3,3-dimethyl-2,3-dihydro-1,2-benzisothiazole 1,1-dioxide,[13] which gave a mixture of mono-**11a** and bis-fluorinated **11b** product which could be separated and individually characterized.

For further analogues with a benzylamine core motif, the preparation proceeded either via hydroxymethylphenyl derivative **7q** or cyanophenyl derivative **7r**. As outlined in Scheme 2, for the former, chlorination using mesyl chloride proceeded in excellent yield and afforded a versatile intermediate that could be reacted with various nucleophiles to afford analogues such as **13a**−**c**. For the latter, reduction of the nitrile in **7r** to give benzylamine derivative **14** in good yield again afforded a useful molecule for further derivatization, such as to sulfonamides **15a**−**c** under standard conditions.

The final series of analogues modified the fused pyrazole ring. These molecules were prepared using methodology similar to those described above but requiring synthesis of the bicyclic pyrazole systems (Scheme 3). Preparation of **18** and regioisomeric **22** was achieved from their corresponding 1,3-diketone precursors **17** and **21** by reaction with hydrazine hydrate. The diketones themselves were prepared under established conditions by reaction of ethyl trifluoroacetate with either tetrahydropyranone **16** or silyl enol ether **20**, respectively. The preparation of the analogous *N*-methylamine precursor **27** was achieved using a similar strategy from BOC-protected piperidinone **24**, via reaction with ethyl trifluoroacetate to afford **25** and then cyclization with hydrazine hydrate to give pyrazole **26**. The BOC group could then be reduced to give the methylamine Ullmann precursor **27**. All three of these intermediates could then be coupled under Ullmann conditions to afford a range of molecules **19a**−**c**, **23a**,**b**, **28**.

Scheme 1. Synthesis of Initial Hit to Lead Analogues[a]

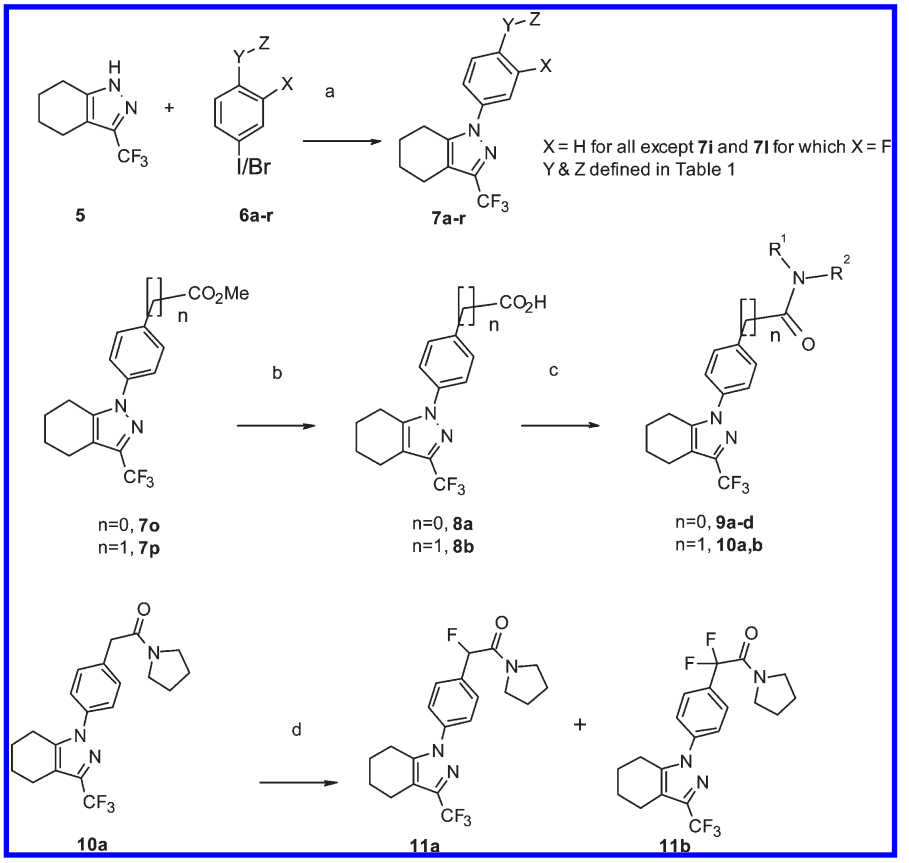

[a] Reagent and reaction conditions: (a) CuI, *trans*-1,2-diaminocyclohexane, K_2CO_3, 1,4-dioxane, 180 °C, microwave; (b) NaOH, EtOH, H_2O, reflux; (c) CDI, CH_2Cl_2, then pyrrolidine (for **9a** and **10a**), piperidine (for **9b**), $PhCH_2CH_2NMeH$ (for **9c**), BuNMeH (for **9d**), or $^cPenNH_2$ (for **10b**); (d) LiN^iPr_2, THF, −78 °C, then 2-fluoro-3,3-dimethyl-2,3-dihydro-1,2-benzisothiazole 1,1-dioxide.

Results and Discussion

We ran our high throughput screen using FLIPR platform methodology on a stable human recombinant GluA2 (flip isoform, unedited) cell line. The ability of test compounds to potentiate glutamate-induced calcium entrance was measured in a dual addition FLIPR protocol with Fluo-4 calcium sensitive probe (see Experimental Section for full details). From this screen output, we selected **7a** as an attractive hit molecule because, despite its lower AMPAR potency, it possessed a superior preliminary developability profile compared to many of the other hits. In particular, **7a** is of relatively low molecular weight and lipophilicity and had an encouraging P450 profile (Table 1). Furthermore, **7a** showed broad selectivity against a range of other ion channels, receptors, and enzymes (data not reported). The clear areas for improvement were identified as solubility and metabolic stability: in particular, **7a** displayed moderate to high turnover in rat and human liver microsomes, consistent with the high hepatic extraction observed in vivo, and low systemic exposure (Table 2). Encouragingly, however, **7a** did exhibit good CNS penetration and had moderate protein binding.

In order to facilitate the hit to lead to development candidate optimization, we designed a screening cascade that maximized the potential for identification of a druglike clinical candidate, including extensive use of physicochemical modeling and profiling, as well as characterization of molecules in both calcium mobilization and electrophysiological techniques. However, in addition to these standard approaches, we sought to make use of the aforementioned published structural data to enable us to consider elements of rational structure-based drug design, which has often been impractical for membrane-bound ion channel targets. To this end, we followed literature precedent and used crystals of the rat GluA2 S1S2 LBD (see Supporting Information for details) to obtain high resolution structures showing the binding mode of a number of compounds. We have solved crystal structures of both the human and rat GluA2 S1S2 ligand binding domain. The residues forming the binding site for positive modulators are the same in rat and human proteins, and binding modes for compounds appear to be identical. We therefore used the rat protein for the structures described in this paper because crystals of the rat protein tended to be of better quality and grew more readily.

We initially determined the X-ray crystal structure of compound **7a** in complex with the rat GluA2 S1S2 LBD and glutamate at 1.55 Å. This showed a single compound binding at the dimer interface occupying the 2-fold axis in a position common to other allosteric positive modulators (Figure 3a).[10,12] For comparison of the binding modes with other AMPAR allosteric modulators, Figure 3 also contains the crystal structures for two widely characterized AMPAR modulators, aniracetam and cyclothiazide. The binding pocket on the dimer interface is an inverted U shape, and in the structure with aniracetam,[10] the compound only occupies the central part of the U (Figure 3e), with pockets at each end of the U being occupied by a cluster of four water molecules. With cyclothiazide, two compounds bind on either side of the 2-fold axis, occupying the two ends of the U and displacing

Scheme 2. Synthesis of Further Analogues in Hit Optimization Phase[a]

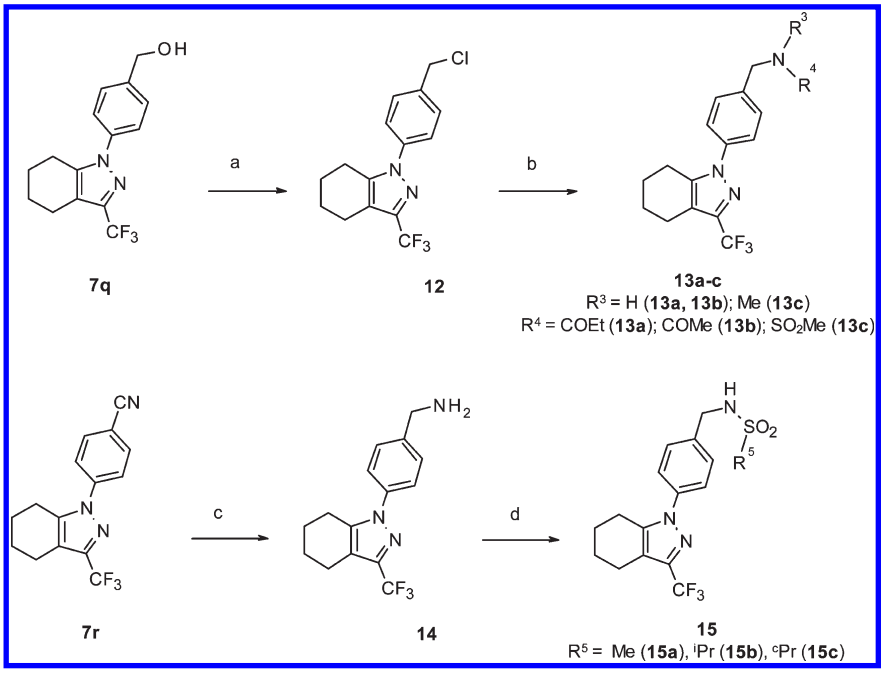

[a] Reagent and reaction conditions: (a) $MeSO_2Cl$, CH_2Cl_2, 94%; (b) R^3R^4NH, DMF, NaH, 0 °C, then **12**; (c) $LiAlH_4$, THF, 85%; (d) Et_3N, R^5SO_2Cl, CH_2Cl_2.

Scheme 3. Synthesis of Analogues Optimizing Pyrazole-Fused Saturated Ring[a]

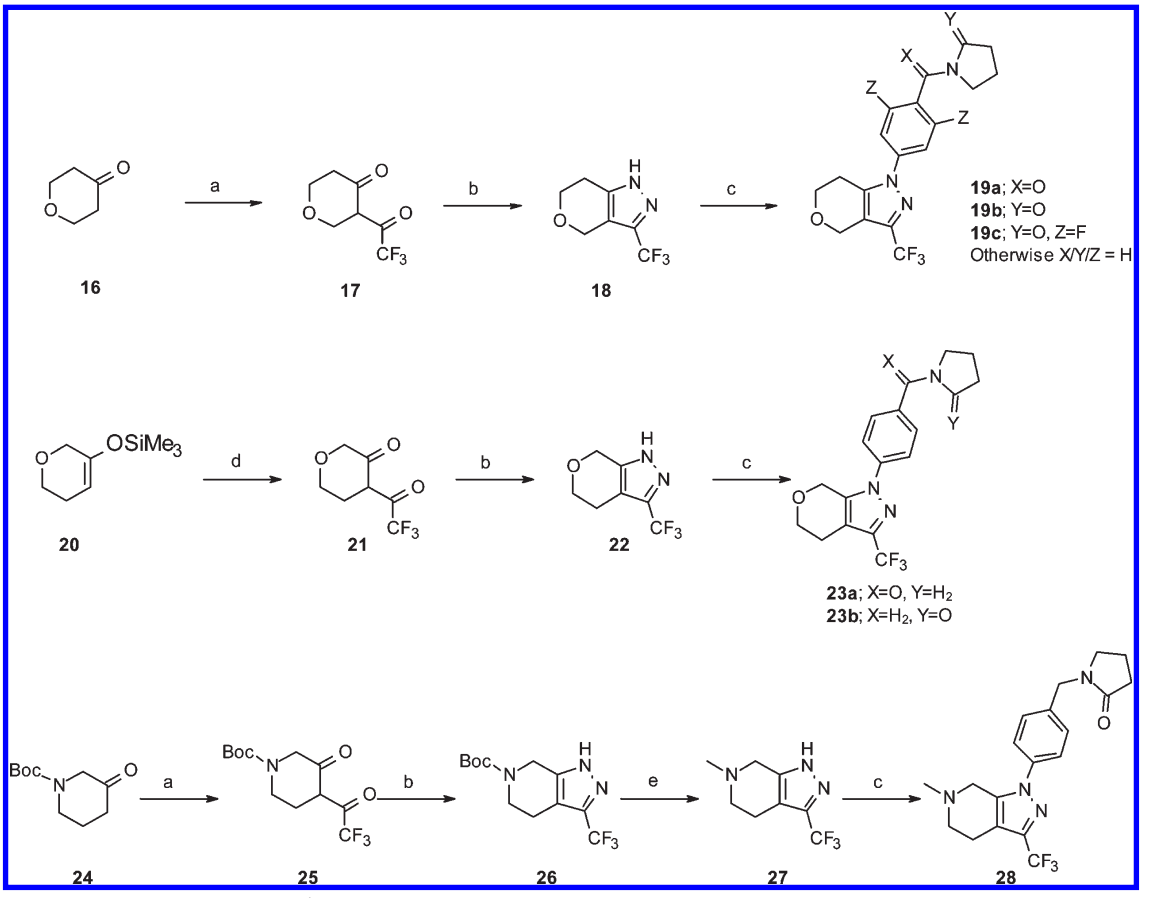

[a] Reagent and reaction conditions: (a) LiN^iPr_2, THF, −70 °C, then $CH_3COCH_2COCF_3$; (b) $N_2H_4.H_2O$, EtOH, 60 °C; (c) substituted phenyl iodide, Cu_2O, $Me_2NCH_2CO_2H$, Cs_2CO_3, DMSO, 130 °C; (d) MeLi, Et_2O, then $CH_3COCH_2COCF_3$; (e) $LiAlH_4$, THF, 58 °C, 71%.

the cluster of four water molecules with a norbornenyl moiety (Figure 3f).[12] The other end of the cyclothiazide extends out of the inverted U shaped cavity toward the solvent region. Analogues of cyclothiazide in which the buried norbornenyl group has been replaced with a cyclopentyl or other groups are less potent.[14,15] In the crystal structure of **7a**, the

Table 1. Biological and in Vitro DMPK Data for Hit to Lead Analogues[a]

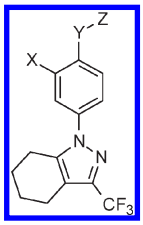

Cpd	X	Y	Z	pEC50	Asym max	MWt	logD [b]	Sol [c]	CYP450 IC50 (μM) [d]	CLi (mL/min/g) [e]	
										Rat	human
7a	H	CO	NMe_2	4.6	94%	337	3.0	138	2D6 6	12.7	3.5
7b	H	CO	morpholine	<4.7	81%	379	3.1	123	>10	<0.5	1.3
9a	H	CO	pyrrolidine	5.0	123%	363	3.0	133	2D6 6	2.4	<0.5
9b	H	CO	piperidine	<4	100%	377	1.6	16	-		
9c	H	CO	$NMeCH_2CH_2Ph$	4.4	84%	427	3.0	57	2C19 3; 2C9 1	25.7	4.4
9d	H	CO	NMeBu	4.8	86%	379	3.2	65	2C9 6; 2D6 8	14.1	1.6
7c	H	SO_2	NMe_2	4.7*	63%	373	3.1	5	2C9 2		
7d	H	CO	Me	4.5	94%	308	3.0	13	1A2 0.1; 2C9 4		
7e	H	none	SO_2Me	4.5	83%	344	3.4	13	1A2 4; 2D6 6		
7f	H	CH_2CO	NMe_2	5.7	107%	351	2.3	118	2C9 7	4.3	8.8
10a	H	CH_2CO	pyrrolidine	5.5	82%	377	3.3	77	2C9 3	14.6	24.9
10b	H	CH_2CO	NH^cPen	4.2*	100%	391	-	0	2C9 0.2; 2D6 8; 3A4 0.7	46.6	>50
7g	H	CHMeCO	pyrrolidine	4.6	81%	391	2.3	59	1A2 6; 2C9 1	18.8	14.1
7h	H	$C(^cPr)CO$	pyrrolidine	4.5	37%	403	3.8	31	2C9 0.3; 2C19 7; 3A4 6	>50	>50
11a	H	CHFCO	pyrrolidine	4.5*	98%	395	3.4	124	>10	19.9	21.1
11b	H	CF_2CO	pyrrolidine	4.7*	94%	395	3.4	124	2C9 4	37.7	40
7i	F	CH_2CO	pyrrolidine	5.9*	79%	395	3.7	41	2C9 7	13.5	6.9
7j	H	CH_2	pyrrolidinone	6.0	132%	363	2.4	110	1A2 1; 2C9 5	2.4	9.1
7k	H	CH_2	NMeCOMe	5.7	94%	351	1.3			3.3	8.3
13a	H	CH2	NHCOEt	5.6	98%	351	3.6	62	1A2 3.5; 2C9 8	11.7	22.4
13b	H	CH_2	NHCOMe	5.9*	79%	337		47	>10 (2D6 not determined)	4.9	4.1
7l	F	CH_2	pyrrolidinone	6.0	112%	381	3.3	88	1A2 2; 2C9 9	2	2.9
7m	H	CH2	COMe	5.4*	111%	322	3.0	44	2C19 2; All others ≤1	5.4	2.6
15a	H	CH_2	$NHSO_2Me$	5.1	112%	373	2.5	103	>10	1.6	<0.7
13c	H	CH_2	$NMeSO_2Me$	4.7*	102%	387	3.3	15	>10	0.9	<0.5
15b	H	CH_2	$NHSO_2{}^iPr$	5.0*	79%	401	2.8	11	>10	2.5	0.8
15c	H	CH_2	$NHSO_2{}^cPr$	5.0*	112%	399	3.2	12	>10	2.5	1.6
7n	H	CH_2		5.0*	118%	399	3.3	12	>10	1.1	<0.5

[a] FLIPR generated pEC_{50} against hGluA2 flip isoform. All values are ±0.2 and $n \geq 3$ (except for $*n = 2$). Asym max is the fitted maximum response, relative to 100% defined as the maximal response of cyclothiazide standard. [b] Measured log *D* values. [c] Kinetic solubility from DMSO stock solution in pH 7.4 phosphate buffered saline. [d] Inhibition of major CYPP450 isoforms; data reported where observed $IC_{50} \leq 10\ \mu M$ against specific isoform. [e] Intrinsic clearance in rat and human liver microsomes.

Table 2. Rat Pharmacokinetic Profiles of Key Indazole Derivatives after a 3 mg/kg Oral Dose

compd	AUC_{0-t}, ng·h/mL	C_{max}, ng/mL	brain:blood AUC_{0-t} ratio	eCLb, [a] (mL/min)/kg	rat plasma protein binding, %	rat brain tissue binding, %	perm, [b] nm/s
7a	78	50	1.3	61	95.2	98.2	
7b	1984	586	1.2	14	97.4	96.8	455
9a	472	228	1.5	12	99.0	99.4	415
7f	262	260	2.8	47	97.8	98.8	
10a	166	95	0.9	55	99.6	98.1	
7i	248	111	0.3	55	99.8	99.4	
7j	231	121	1.4	54	98.4	99.4	
15a	416	197	1.6	43	97.9	99.2	335
7n	364	136	2.5	41	96.8	99.5	400
7l	331	167	1.3	47	98.9		420

[a] Estimated clearance value (eCLb) based on in vivo hepatic extraction determined following a 3 mg/kg oral dose and blood sampling via the hepatic portal vein and heart and using 85 (mL/min)/kg as liver blood flow in rat. [b] Artificial membrane permeability (perm) assay.

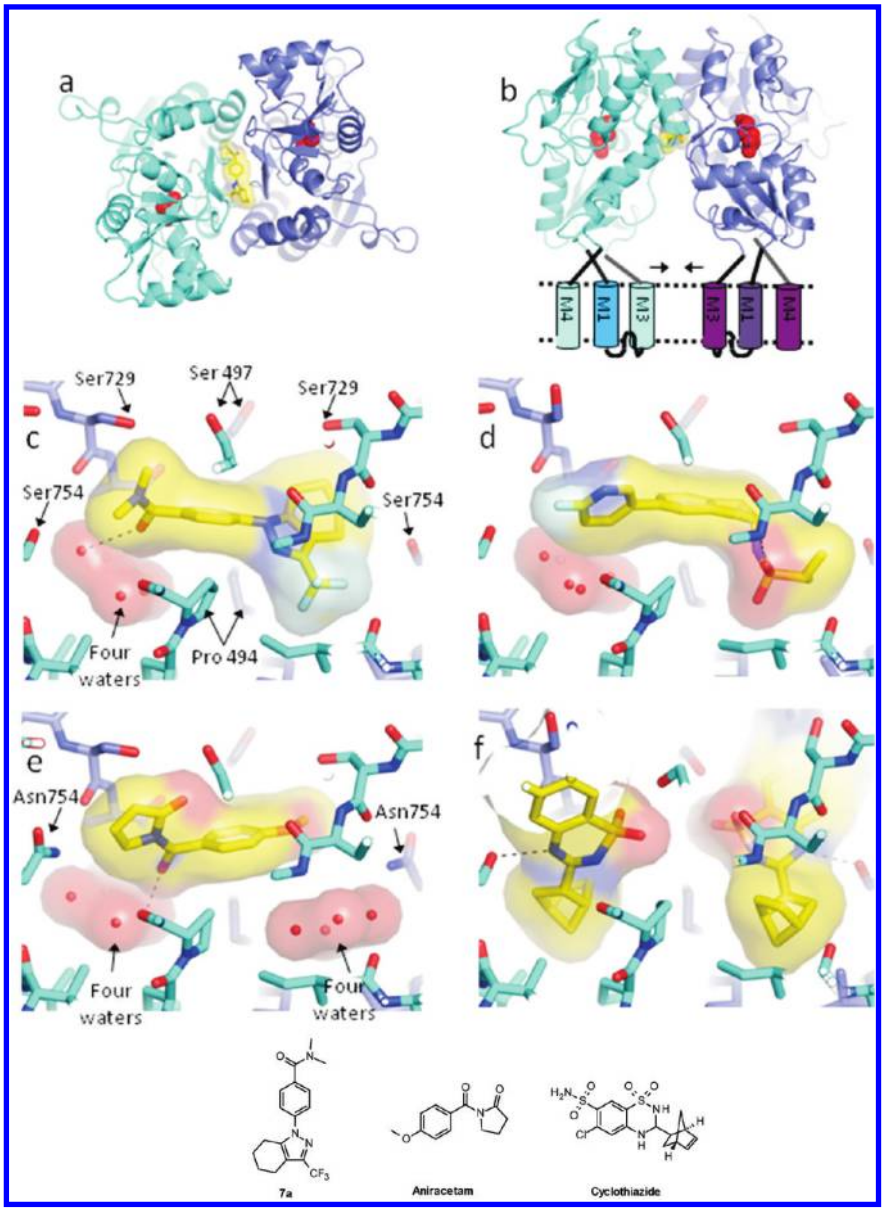

Figure 3. (a, b) Orthogonal views of the 1.55 Å structure of **7a** (**7a** is in yellow, glutamate in red). (b) For orientation, schematic of the ion channel is shown in an open state. The directions of the arrows indicate directions of movement for closure. (c−f) Comparison of the binding mode of **7a** (c) with other allosteric modulators. (d) **4** in complex with the human GluA2 S1S2 LBD.[5] (e) Aniracetam (PDB code 2al5). (f) Cyclothiazide (PDB code 1lbc). The binding pocket resembles an inverted U. In the aniracetam structure (e) both ends of the pocket are occupied by a cluster of four water molecules (small red spheres). H-bonds are indicated by dotted lines.

trifluoromethyl group occupies one end of the U shaped cavity (Figure 3c), sitting in a position similar to that of the norbornenyl group in cyclothiazide and an isopropyl sulfonamide in the structure of our previous development molecule **4**

with the human GluA2 S1S2 LBD (Figure 3d).[8] The phenyl moiety of **7a** sits on the 2-fold axis making hydrophobic interactions with Pro 494 (Figure 3c), while the carbonyl moiety of the compound points down into the other arm of the inverted U to make a single hydrogen bond with one of the four waters in the pocket. While there are a number of serine residues surrounding the binding pocket, compound **7a** makes no obvious hydrogen bonds with the protein. However, there is a 2.9 Å contact from the main-chain NH function of Gly 731 to one of the fluorine atoms of **7a**, suggesting this fluorine might be acting as an unusual hydrogen bond acceptor.[16] The trifluoromethyl group of **7a**, which has displaced the cluster of four waters, also makes van der Waals interactions with residues Leu 751 and Ile481 and the carbonyl backbone of Lys493. While the tetrahydroindazole ring is also largely buried in the pocket, the upper part (oriented as in Figure 3c) makes contact with solvent, suggesting that limited substitutions would be tolerated at this position. More usefully, however, the terminal dimethylamide group of compound **7a**, sitting above four water molecules at one end of the inverted U shaped pocket, was in a position that looked as though there was greater potential for ligand modification to reach Ser729, Ser754, and the waters in the pocket as potential hydrogen bonding partners.

From this understanding of the interaction of **7a** with the LBD and from the data reported above, we initiated a program of hit optimization to improve principally metabolic stability but also potency and solubility. To measure potency, we used the same assay reported for the high throughput screen, using fluorescent calcium-indicator dyes with FLIPR methodology. For this screen, the biological test system selected was the GluA2 homomeric AMPA receptor, and a concentration response curve was derived for potentiation of glutamate-induced rises in intracellular calcium and analyzed relative to a known positive standard control (see Experimental Section for full details). Additionally, molecules of interest were also profiled using whole cell patch clamp electrophysiology, measuring glutamate-evoked current recorded from both human GluA2 flip unedited HEK293 cells and rat cortical neurons. Further data (not included in article) also confirmed, for those molecules studied, a broad spectrum positive modulatory activity across AMPARs formed from different subunits (GluA1, GluA3, and GluA4 homomers) and also equivalent potency at rat and human GluA2 flip homomeric AMPARs.

We reasoned that a likely cause of the metabolic instability of parent hit **7a** was the terminal dimethylamide group and, as such, prepared cyclic derivatives morpholine **7b**, pyrrolidine **9a**, and piperidine **9b**. Interestingly, as shown in Table 1, the potency of these analogues was dependent on the amine ring size; five-membered pyrrolidine derivative **9a** was more active than **7a**, and both six-membered morpholine **7b** and piperidine **9b** derivatives were significantly less active. Very encouragingly, however, for **9a** and even more so for **7b**, the metabolic stability had increased significantly in both rat and human microsomes. These molecules were progressed to evaluation in a rat pharmacokinetic study (Table 2) which confirmed the lower in vivo clearance and validated the earlier hypothesis of the likely cause of rapid turnover of **7a** in vitro. Furthermore, these molecules showed acceptable or no inhibition of P450 isoforms, although the solubility was consistently low in line with the original dimethylamide. Although these pharmacokinetic data were very promising, we struggled to maintain this improvement and retain or improve potency at the AMPAR. For instance, other acyclic amides **9c** and **9d** investigated gave similar potencies to the initial hit but with increased intrinsic clearances, potentially contributed to by their higher lipophilicities.

Given the difficulties inherent in balancing the potency with the pharmacokinetic profile, we decided to investigate alternatives to the amide. Replacing the carbonyl with a sulfonyl group as in sulfonamide analogue **7c** gave equivalent potency but lower solubility. Removal of the nitrogen atom to give either acetophenone derivative **7d** or methyl sulfone derivative **7e** again did not improve AMPAR potency and led to a lower solubility and also further inhibition of P450 isoforms, particularly for ketone **7e**.

One strategy to improve the solubility was to enhance flexibility by introduction of a linker atom between the phenyl ring and the amide. The initial analogue **7f**, which is the homologue of hit **7a**, gave a very interesting profile: potency had been significantly increased; however, in vitro stability was not improved. The next analogues to be prepared sought to combine the improved metabolic stability of cyclic amides **7b** and **9a** with the improved potency of **7f**. However, key hybrid analogue **10a**, while maintaining an improved potency, gave lower metabolic stability, confirmed by the higher in vivo clearance and slightly lower systemic exposure relative to **7f**.

In order to allow more rational design of subsequent analogues, we generated ligand-bound crystal structures of a number of analogues. To exemplify this, Figure 4 shows the binding mode for **10a** from a 1.5 Å crystal structure with the rat GluA2 S1S2 LBD, highlighting the space available for substitution. From these crystal structures, we were able to create computational docking models to allow us to prioritize future targets and so avoid those likely to lead to unfavorable interactions with the protein, such as substitution of the central phenyl ring.

Given our additional information from the high resolution structure of **10a** bound into the GluA2 S1S2 protein construct and given that we had already achieved a good pharmacokinetic profile in **9a** and **7b**, we reasoned that we should be able to design appropriately substituted homologated analogues to improve both PK and potency over hit **7a**. Moving from tertiary amide **10a** to related secondary amide **10b** gave a significantly lower potency and solubility and a worse P450 inhibition and microsomal stability profile. We attempted to block a likely site of metabolism on the benzylic methylene spacer unit by introduction of either alkyl or fluorine groups. Specifically, monomethyl analogue **7g** and cyclopropyl substituted analogue **7h** were unsuccessful, again reducing potency and metabolic stability. The mono- and bis-fluorinated products **11a** and **11b** gave an identical pattern with a detrimental impact on potency and intrinsic clearance relative to **10a**. In addition to creating a potentially vulnerable site of benzylic oxidation, insertion of the methylene between the amide and phenyl rings also increases the electron density of the phenyl ring. However, analysis of the protein structure around the phenyl ring in the structures solved indicated that larger substitution would unlikely be tolerated; so to understand if metabolic stability could be restored by analogues with lower aromatic electron density, we restricted the investigation to fluorination of the central benzene ring. Fluorophenyl derivative **7i** (fluorine meta to indazole on phenyl ring) was prepared, for which data were encouraging: higher potency and a clean P450 profile relative to **10a**, in addition to slightly improved human microsomal metabolic stability.

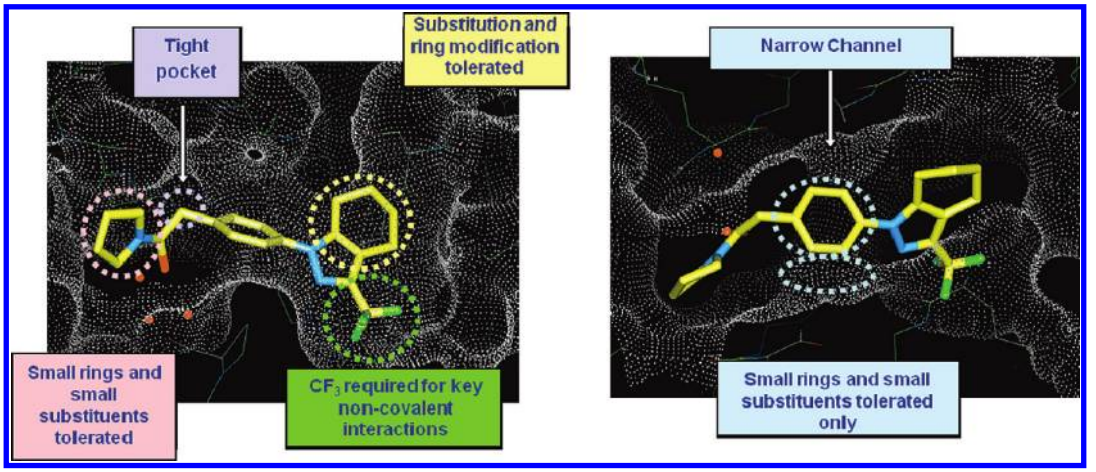

Figure 4. Detail of the binding site of **10a**, from a 1.5 Å crystal structure. The surface of the protein is represented by dots. Picture is generated by Quanta (Accelrys Software Inc.).

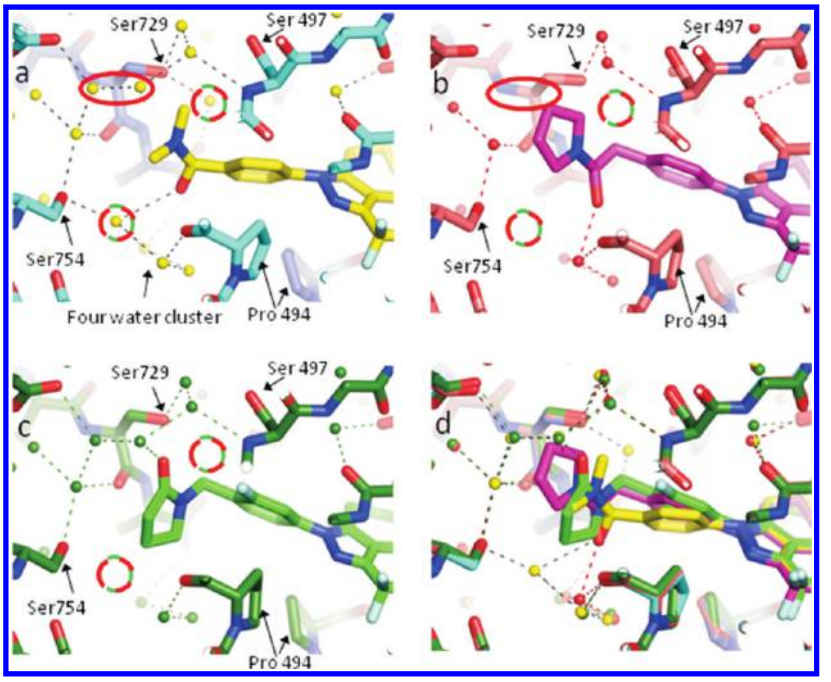

Figure 5. Comparison of (a) the 1.55 Å crystal structure of **7a** (pEC_{50} = 4.6), (b) the 1.5 Å crystal structure of **10a** (pEC_{50} = 5.5), and (c) the 1.97 Å crystal structure of **7l** (pEC_{50} = 6.0). In (d) the structures are shown superposed; waters are shown as small spheres. Compared with **7a**, compound **10a** has displaced four waters and compound **7l** has displaced two waters (displaced waters indicated by circles). Both **10a** (b) and **7l** (c) have displaced a water molecule that interacted with Ser754. In the Flop isoform of GluA2 residues 754 is a larger asparagine residue.

In order to maintain the methylene spacer that afforded improved potency, we prepared a series of reversed amide derivatives with an embedded benzylamine core motif. The first of these, pyrrolidinone **7j**, gave excellent potency; however, it was still subject to moderate to high in vivo clearance and low to moderate systemic exposure (Table 2) despite the reduced rat intrinsic clearance. Further reversed analogues were investigated including tertiary acyclic **7k** and secondary **13a** and **13b** amides. All of these maintained good potency and had generally adequate P450 profiles, although intrinsic clearance remained moderate, with the larger ethyl amide substituent in **13a** leading to lower metabolic stability than its methyl analogue **13b**. Attempts were also made in this reversed amide series to introduce the fluorine onto the phenyl ring, preparing **7l**, the fluorophenyl analogue of **7j**. This substitution reduced the intrinsic clearance, particularly in human microsomes, leading to a slightly improved pharmacokinetic profile in rat, although still not achieving the concentrations observed for early analogue **7b**. We attempted to rationalize the potency data by analysis of further ligand-bound X-ray structures. In particular, given the increase in compound potency observed from **7a** to **10a** and **7l**, analysis of their structures (Figure 5) showed displacement of different numbers of water molecules from the binding site by both **7l** and **10a** compared with **7a**. Compound **7l** (pEC_{50} = 6.0), which displaced two additional buried waters to **7a**, was more active than **10a** (pEC_{50} = 5.5) which in addition to displacing these additional two buried waters also displaced two further solvent exposed waters. Although the computational docking models were very useful in predicting which compounds could be accommodated in the binding site, affinities were not predictable. The most pragmatic approach was to explore a range of analogues to exploit the seemingly promiscuous nature of this part of the binding site.

Further analogues were sought, as before, to replace the amide functionality, leading to homologated ketone derivative **7m** and sulfonamides **15a**−**c**, **13c**, and **7n**. The ketone was particularly unsuccessful, maintaining high intrinsic clearance but giving a marked worsening in the P450 inhibition profile. The sulfonamides were more encouraging, all giving clean P450 profiles and low intrinsic clearance, although, other than for secondary sulfonamide **15a**, they generally displayed lower solubility. Potencies were also lower than for the analogous amide molecules. Nonetheless, sulfonamides **15a** and **7n** were progressed to evaluation in the rat but disappointingly gave moderate clearance with only slight improvement in oral exposure.

From the highly variable in vitro and in vivo clearance values obtained for a number of analogues, it appeared evident that a better understanding of the metabolic vulnerabilities of the series was necessary. A number of iterations from **7b** and **9a** had failed to combine the desired PK and potency parameters, so we selected several compounds for in vitro metabolite identification studies to improve understanding of the vulnerable sites within our lead series' molecules, including **7l**, **10a**, and **11b**. The results from this indicated that one of the major sites of metabolism appeared to be the aliphatic part of the tetrahydroindazole ring. However, it also appeared that the Z group and the linker Y (as defined in Table 1) were important determinants of metabolic vulnerability, perhaps explaining some of the variability in clearance observed.

We found that some of the compounds studied, including **7l**, were metabolized by hydroxylations of both the tetrahydroindazole and the Z group. Compound **10a** only appeared to undergo hydroxylation of the tetrahydroindazole. In contrast, **11b** was completely metabolized but with only trace levels of a putative hydroxylated metabolite detected; in this case it is believed that metabolism was directed mainly toward hydrolysis of the amide, driven by the fluorines on the benzylic carbon markedly increasing the susceptibility of the adjacent carbonyl group to nucleophilic attack.

The conclusions from the metabolite identification studies were that benzylic fluorination should be avoided and that investigation into ways to stabilize the aliphatic part of the tetrahydroindazole group by, for example, introduction of heteroatoms should be carried out.

From this understanding and from analysis of the structural information, we sought to prepare analogues that introduced heteroatoms into the saturated ring of the tetrahydroindazole. Our structural data confirmed that these changes should be tolerated but also indicated that the binding pocket would probably not accommodate a large additional substituent. Furthermore, as all our crystal structures had identified the binding interaction with the trifluoromethyl group as the key interaction with the protein, we avoided modification of this conserved functional motif. Consequently, the analogues targeted replaced one of the distal methylene carbons in the fused ring with either a nitrogen or oxygen heteroatom.

Encouragingly, as shown in Table 3 the set of molecules prepared had broadly improved profiles with excellent in vitro properties: high permeability, low intrinsic clearance in rat and human microsomes, and generally low potential for inhibition of major human CYP P450 isoforms Furthermore, the introduction of the heteroatom into the tetrahydroindazole ring generally improved solubility, lowered log D, and consequently considerably reduced protein binding measured against either plasma or brain tissue homogenate. Most encouragingly, from evaluation of the pharmacokinetics in rat, the molecules generally showed good oral exposure and lower in vivo clearance relative to their tetrahydroindazole analogues; CNS penetration also remained consistently high (not shown).

All of these molecules were selected for downstream progression, together with those molecules previously profiled in vivo with the best exposure in rat (generally blood AUC_{0-t} > 400 ng·h/mL), thus allowing us a range of solubility, protein binding, and physicochemical parameters in the molecule set.

These molecules were profiled in electrophysiology, selectivity, developability, and early toxicology screens, and from these a small set of molecules were identified that were suitable for further evaluation as potential development candidates. All five molecules listed in Table 4 showed excellent wider selectivity against a wide range of other ion channels (including hERG, NMDA, and kainate channels), enzymes, and GPCRs. Furthermore, as exemplified for one example in Figure 6, analogues showed clear potentiation of AMPA currents in whole cell patch clamp electrophysiology evaluation of the recombinant hGluA2 cell line and also in rat neuronal cells.

Having demonstrated clear potentiation of AMPAR-mediated currents in both recombinant hGluA2 and rat cultured neurones, we assessed this set of molecules in the key side effect profiling model, the maximum electroshock threshold (MEST) test. In the MEST test, corneal application of electrical current (CC_{50} of approximately 60−70 mA, 0.1 ms duration) in the rat induces tonic and full tonic−clonic seizures. In order to assess the potential of these molecules to reduce seizure threshold activity, male Lister Hooded (LH) rats were pretreated with compound, saline vehicle, or picrotoxin as a positive control 30 min before testing. Mean blood and brain concentrations were measured from satellite rats, sampled immediately after testing. None of the molecules investigated significantly reduced seizure threshold, showing a lack of proconvulsant activity in this test and contrasting with the profiles of a number of AMPAR positive modulators reported in the literature (internal data not presented). Further evaluation of **15a** identified that it had a poor pharmacokinetic profile in the dog with high blood clearance observed approximating to that of liver blood flow and only moderate bioavailability (Fpo 18%). **15a** was also found to be mutagenic in preliminary AMES evaluation. All remaining four molecules were clean in preliminary genotoxicity screens and were profiled in the passive avoidance task,[17] in which scopolamine administration (0.8 mg/kg, intraperitoneal) at 6 h post-training rendered experimentally naive male Wistar rats (n = 6−12/group) amnesic when tested 24 h later. As highlighted in Table 4, **9a**, **19a**, and **19c** (administered in 1% methyl cellulose solution 30 min prior to test) attenuated the scopolamine-induced amnesic deficit with significant effects at 10 and 30 mg/kg for **9a** and 30 mg/kg for **19a** and **19c** (no concentration data available). **7b** showed no effect in this model. Furthermore, all the compounds administered in the absence of scopolamine had no effect on recall of the passive avoidance response or any effect on locomotor activity as assessed in an open field arena.

The successful molecules were subsequently evaluated in a further behavioral model of cognition, novel object recognition (NOR),[18] in which they were tested for their ability to improve a 24 h delay-induced deficit in a test of recognition memory in male Lister Hooded rats (n = 9−12/group). From

Table 3. Characterisation of Indazole Derivatives Containing Heteroatoms[a]

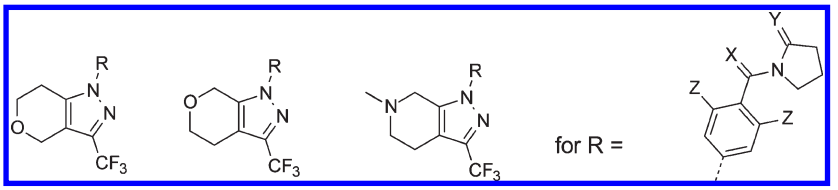

Cpd	Pyrazole	X	Y	Z	pEC50	Asym max	logD [b]	Bl AUC [c] ng.h/mL	Bl Cmax [c] ng/mL	CLb [d] mL/min/kg	rPPB %	rBTB %	Perm [e] nm/s	Sol [f]	CYP P450 IC50 μM [g]	CLi (n rat
19a		O	H_2	H	<4.7	81%	2.4	1329	551	e6	86.3	88.4	495	192	>10	0.9
19b		H_2	O	H	5.0	138%	2.4	972	808	e41	84.0	87.9	470	215	>8	0.8
19c		H_2	O	F	4.7	120%	2.5	481	76	e22	93.6	96.3	470	207	>10	0.6
23a		O	H_2	H	4.0	75%	2.6	733	225	e13	93.3	95.5	490	104	>10	0.8
23b		H_2	O	H	5.3	116%	2.6	824	331	ND	94.3	94.9	440	123	>10	<0.5
28		H_2	O	H	4.4	102%	2	294	131	e22	85.8	63.0	430	93	>10	<0.5

[a] FLIPR generated pEC_{50} against hGluA2 flip isoform. All values are ±0.2 and $n \geq 3$. Asym max is the fitted maximum response relative to 100% defined as the maximal response of cyclothiazide standard. [b] Measured log *D* values at pH 7.4. [c] Blood AUC_{0-t} values following 3 mg/kg oral dose. [d] e = estimated clearance value based on in vivo hepatic extraction determined following a 3 mg/kg oral dose and blood sampling via the hepatic portal vein and heart and using 85 (mL/min)/kg as liver blood flow in rat. [e] Artificial membrane permeability assay. [f] Kinetic solubility from DMSO stock solution in pH 7.4 phosphate buffered saline. [g] Inhibition of major CYPP450 isoforms, data reported where observed $IC_{50} \leq 10$ μM against specific isoform. [h] Intrinsic clearance in rat and human liver microsomes.

Table 4. Characterisation of Indazole Derivatives Containing Heteroatoms[a]

compd	MEST dose tested (brain concn)	passive avoidance	NOR dose (brain concn)
9a	30 mg/kg (4686 ng/g)	10 and 30 mg/kg	0.1 mg/kg* (9 ng/g) 0.3 mg/kg* (19 ng/g) 1 mg/kg* (97 ng/g) 3 mg/kg (542 ng/g)
15a	150 mg/kg (5074 ng/g)		
7b	150 mg/kg (7168 ng/g)	inactive	
19a	150 mg/kg (22525 ng/g)	30 mg/kg	1 mg/kg (228 ng/g) 3 mg/kg (983 ng/g) 10 mg/kg (2609 ng/g)
19c	150 mg/kg (8988 ng/g)	30 mg/kg	0.3 mg/kg (22 ng/g) 1 mg/kg (79 ng/g) 3 mg/kg (386 ng/g) 10 mg/kg (1413 ng/g)

[a] Assessment in MEST at given dose (brain concentrations measured in satellite animals at MEST measurement time). Passive avoidance tested at 3, 10, 30 mg/kg and active doses reported (brain concentrations not measured). NOR doses tested with those producing significant cognitive improvement labeled with ∗ (brain concentrations measured in study animals at completion of NOR test).

this evaluation, only **9a** gave an acceptable profile, showing potent procognitive activity at low concentrations.

Detailed Evaluation of the Preclinical Profile of 9a. Development candidate **9a** exhibited low solubility in water, simulated gastric fluid and fasted simulated intestinal fluid (34−86 μg/mL over 24 h), and moderate solubility in fed simulated gastric fluid (364−391 μg/mL over 24 h), with high stability in all media tested and as a solid on prolonged evaluation. In vitro, **9a** showed low potential for direct inhibition of the major human CYP450s 1A2, 2C9, 2C19, 2D6, and 3A4 and was not a metabolism-dependent inhibitor of CYP2D6 and CYP3A4. Furthermore, **9a** had high passive permeability (405 nm/s) in the artificial membrane permeability assay and was not a P-glycoprotein (P-gp) substrate. Following single intravenous administration of **9a**, the volume of distribution at steady state (V_{ss}) was greater than total body water in all species tested, indicating a good tissue distribution (Table 5). However, blood clearance (CLb) was moderate in rat and high in other species, resulting in relatively short terminal half-lives of between 0.5 and 1.6 h . Mean oral bioavailability was moderate in rat (54%) and low in all other species tested (≤20%), largely reflecting the moderate to high clearance. Oral absorption was fairly rapid with the T_{max} between 0.5 and 1 h in all species tested.

The intrinsic clearance of **9a** was determined in microsomes and in cryopreserved (rat, dog, minipig, monkey, and human) hepatocytes (Table 6). There was general agreement

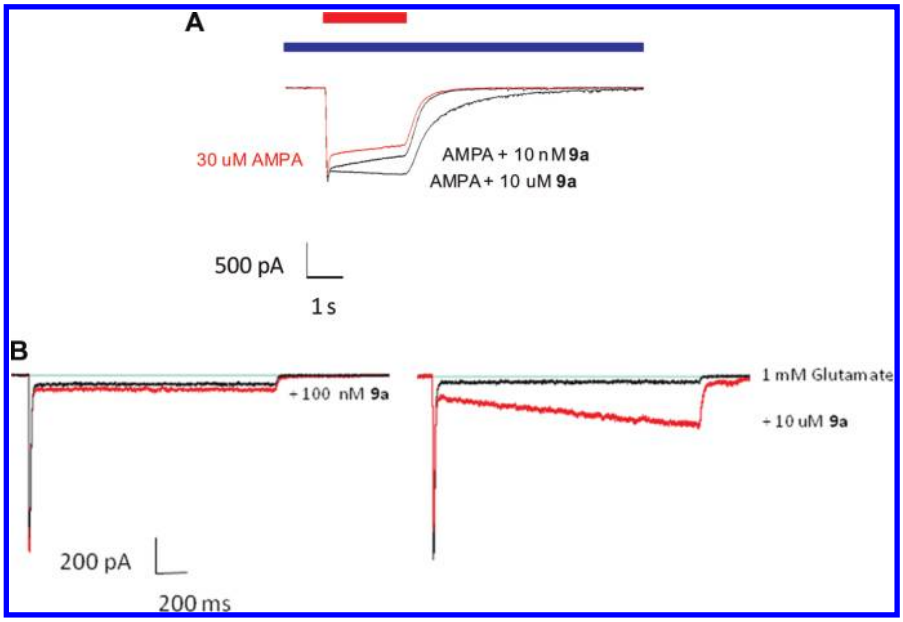

Figure 6. Electrophysiological activity of lead analogues. (A) Representative traces recorded from rat cultured hippocampal neurons. The red bar above the traces illustrates 2 s period of 30 μM AMPA application; associated current trace is also in red. The blue bar illustrates application of **9a** at either 10 nM or 10 μM. Quantified increases in charge transfer (measured area under the curve) are as follows: 10 nM, 37 ± 9%; 10 μM, 62 ± 15%. (B) Representative whole cell current traces recorded from HEK293 cell expressing hGluA2i homomeric AMPARs. Control currents evoked by application of 1 mM glutamate are in black, and currents evoked by **9a** applied at 100 nM (left panel) and 10 μM (right panel) are in red. Quantified increases in charge transfer (measured area under the curve) are as follows: 100 nM, 21 ± 7%; 10 μM, 600 ± 40%.

Table 5. Pharmacokinetic Parameters for **9a** Obtained in Male Rat, Dog, Minipig, and Monkey after Intravenous and Oral Administration[a]

parameter	rat	dog	minipig	monkey
strain, sex	Sprague−Dawley, male	Swiss Beagle, male	Gottingen, male	Cynomolgus, male
n	3	3	3	3
dose (mg/kg)	iv 2.5	iv 0.25	iv 0.5	iv 0.25
	po 3	po 0.5	po 1	po 1
blood clearance ((mL/min)/kg), *% liver blood flow*[b]	40 [34−44] *47%*	32 [31−36] *100%*	23 [16−32] *77%*	38 [30−44] *86%*
V_{ss} (L/kg)	4.8 [4.0−5.7]	3.4 [2.8−4.5]	3.2 [2.0−5.2]	1.6 [1.2−1.9]
iv half-life ($t_{1/2}$) (h)	1.4 [1.2−1.5]	1.3 [0.9−2.1]	1.6 [1.3−1.9]	0.5 [0.5−0.6]
oral bioavailability (%)	54 [44−64]	12, 24 (n = 2)	13 [6−20]	2 [1−3]
oral C_{max} (ng/mL)	245 [153−320]	14, 24 (n = 2)	29 [11−57]	5 [3−6]
oral T_{max} (h)	0.5 [0.5−0.5]	0.6, 0.6 (n = 2)	0.5 [0.3−4.0]	1.0 [1.0−1.3]
oral half-life ($t_{1/2}$) (h)	2.3 [1.2−3.2]	0.9, 1.0, (n = 2)	4.5 [1.7−9.6]	1.4 [1.0−2.2]

[a] All parameters were calculated from blood concentration−time data. All data are reported as mean [and range]. For T_{max} the median [and range] are given. [b] Calculated using the following liver blood flows ((mL/min)/kg): rat 85, dog 31, minipig 30, cynomolgus monkey 44.

Table 6. Intrinsic Clearance (CLi) of **9a** in Liver Microsomes and in Cryopreserved Hepatocytes (70 000 cells/mL) Obtained from Preclinical Species and Human

	CLi [(mL/min)/(g of liver)]				
	rat	dog	monkey	minipig	human
liver microsomes (n = 3)[a]	2.4 [2.4−2.5]	1.3 [1.2−1.7]	12 [11.5−12.2]	4.4 [3.8−4.5]	< 0.5 [< 0.5−0.8]
cryopreserved hepatocytes (n = 1, unless otherwise stated)	2.3	2.6	> 50	7	1.2 (n = 1), 0.7 (n = 3)

[a] Values represent median and [range] from n = 3 determinations.

between the microsomal and hepatocyte CLi values with low to moderate values obtained for human and the highest CLi values for minipig and monkey. With the exception of dog, correlation of in vitro CLi with in vivo CLb was generally good, suggesting that in vivo clearance in human is likely to be low to moderate.

Development candidate **9a** exhibited no evidence of genotoxic potential in the in vitro predevelopment genetic toxicity screens. Furthermore, a hERG assay demonstrated that **9a** at a nominal concentration of 10 μM (equivalent to 3.6 μg/mL) was found to have no significant inhibitory effect on hERG tail current recorded from stably transfected cells. **9a** was successfully evaluated in single and repeat dose oral toxicity studies of up to 4 weeks in duration in Sprague−Dawley rats and beagle dogs, allowing a very wide margin between predicted efficacies and no adverse event level for future clinical exploration.

The binding mode for **9a** was confirmed by crystallography to be similar to that seen for other compounds with differences in the water network on the 2-fold axis seemingly caused by a reorientation of the carbonyl moiety of **9a** compared to **7a** (Figure 7). A 1.6 Å crystal structure of **19b** (data not shown) again had a very similar binding mode.

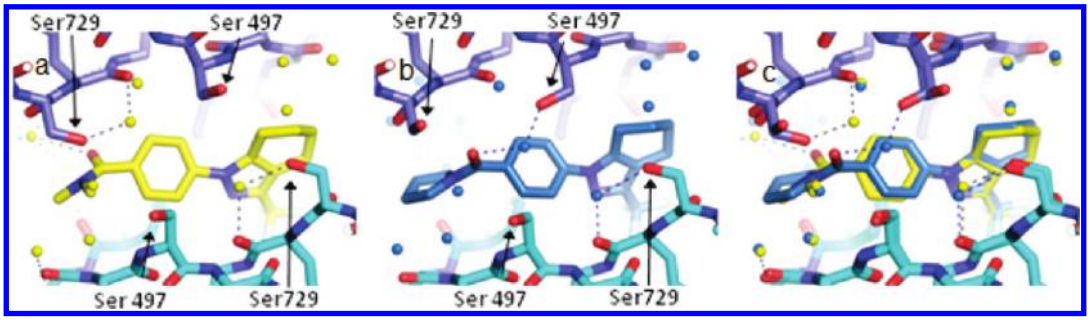

Figure 7. View down the 2-fold axis comparing: (a) the 1.55 Å crystal structure of **7a** with (b) the 2.2 Å crystal structure of **9a** ((c) overlaid image of **7a** and **7b**). Waters are shown as small spheres. Some hydrogen bonds are indicated with dotted lines. In the structure of **9a** the carbonyl is pointing out of the plane of the figure and makes an interaction with a water molecule close to the 2-fold axis of the dimer.

Conclusions

Starting from a good quality hit from a high throughput screen, we were able to optimize the pharmacokinetic properties to deliver a range of molecules with attractive developability profiles. This optimization was facilitated by the regular generation of ligand-bound X-ray crystal structures, allowing focused exploration of chemical space to reduce the number of analogues required to arrive at the development candidate. This work has uncovered a novel chemotype of AMPAR positive allosteric modulator that binds into the pocket common to all known modulators but with a unique and highly conserved mode of interaction. Development candidate **9a** is a potently efficacious molecule with an attractive safety profile in preclinical species.

Experimental Section

Chemistry. General Remarks. Starting materials were obtained from commercial suppliers and used without further purification unless otherwise stated. Flash chromatography was carried out using prepacked Isolute Flash or Biotage silica gel columns as the stationary phase and analytical grade solvents as the eluent. Catch and release purification was carried out using SCX (strong cation exchanger) cartridges consisting of bonded-phase silica with sulfonic acid functional groups. Mass directed preparative HPLC was carried out using a 19 mm × 100 mm or 30 mm × 100 mm, 5 μm, reversed phase Waters Atlantis column as the stationary phase and a gradient from water + 0.1% formic acid to acetonitrile + 0.1% formic acid as the eluent. The eluent was monitored by a Waters 996 photodiode array and a Micromass ZQ mass spectrometer. All yields reported are of purified, isolated material. NMR spectra were obtained at 298 K at the frequency stated using either a Bruker DPX400 or an Oxford Instruments 250 MHz machine and run as a dilute solution of $CDCl_3$ unless otherwise stated. All NMR spectra were referenced to tetramethylsilane (TMS δ_H 0, δ_C 0). All coupling constants are reported in hertz (Hz), and multiplicities are labeled s (singlet), bs, (broad singlet), d (doublet), t (triplet), q (quartet), dd (doublet of doublets), dt (doublet of triplets), and m (multiplet).

Purity was determined by LCMS (liquid chromatography/mass spectrometry) using an Agilent 1100 HPLC system with a 4.6 mm × 50 mm, 3 μm, reversed phase Waters Atlantis column as the stationary phase. A gradient elution from 97% water + 0.05% formic acid/3% acetonitrile + 0.05% formic acid to 97% acetonitrile + 0.05% formic acid over 3 min plus a further minute continuing this mixture at a flow rate of 1.5 mL/min was used as the eluent. Retention time is reported as minutes (with percentage intensity for DA/ELSD for the relevant peak). Spectroscopic monitoring was performed using an Agilent 1100 diode array (DA) detector or a Sedex evaporative light scattering detector (ELSD). Total ion current traces were obtained for electrospray positive and negative ionization (ES+/ES−) and atmospheric pressure chemical positive and negative ionization (AP+/AP−). All final products were of > 95% purity by HPLC unless otherwise stated. For all key molecules, high resolution mass spectrometry data were acquired as accurate mass centroided data using a Micromass Q-Tof 2 hybrid quadrupole time-of-flight mass spectrometer equipped with a Z-spray interface.

General Procedure for Ullmann Coupling Reactions To Prepare 7a−r. A mixture of **6** (0.36 mmol), 3-(trifluoromethyl)-4,5,6,7-tetrahydro-1*H*-indazole (0.44 mmol), copper(I) iodide (1 mol %, 0.0036 mmol), *trans*-1,2-diaminocyclohexane (10 mol %, 0.036 mmol), and potassium carbonate (0.76 mmol) in 1,4-dioxane (0.5 mL) was stirred at 180 °C in a microwave reactor for 15 min. Then fresh copper(I) iodide (1 mol %, 0.0036 mmol) and *trans*-1,2-diaminocyclohexane (10 mol %, 0.036 mmol) were added, and the mixture was stirred at 180 °C in a microwave reactor for 20 min. The reaction mix was cooled and added to a 5 g prepacked silica column which was then eluted from ethyl acetate. The product was further purified by mass directed autoprep to give the required product.

***N*,*N*-Dimethyl-4-[3-(trifluoromethyl)-4,5,6,7-tetrahydro-1*H*-indazol-1-yl]benzamide (7a).** Yield 43%. LCMS (ES+) *m*/*z* found 338, retention time 3.09 min. $C_{17}H_{18}F_3N_3O$ requires 337. ^{1}H NMR (400 MHz, $CDCl_3$): 1.83 (4H, m), 2.70 (4H, m), 3.00 (3H, s), 3.14 (3H, s), 7.54 (4H, m). HRMS (ES+) *m*/*z* 338.1465 ($[M + H]^+$ calcd for $C_{17}H_{19}F_3N_3O^+$ 338.1480).

1-[4-(4-Morpholinylcarbonyl)phenyl]-3-(trifluoromethyl)-4,5,6,7-tetrahydro-1*H*-indazole (7b). Yield 82%. LCMS (ES+) *m*/*z* found 380, retention time 3.07 min. $C_{19}H_{20}F_3N_3O_2$ requires 379. ^{1}H NMR (400 MHz, $CDCl_3$): 1.84 (4H, m), 2.71 (4H, m), 3.36−3.90 (8H, m), 7.53 (2H, m), 7.58 (2H, m). HRMS (ES+) *m*/*z* 380.1569 ($[M + H]^+$ calcd for $C_{19}H_{21}F_3N_3O_2^+$ 380.1586).

***N*,*N*-Dimethyl-2-{4-[3-(trifluoromethyl)-4,5,6,7-tetrahydro-1*H*-indazol-1-yl]phenyl}acetamide (7f).** Yield 21%. LCMS (ES+) *m*/*z* found 352, retention time 3.15 min. $C_{18}H_{20}F_3N_3O$ requires 351. ^{1}H NMR (400 MHz, $CDCl_3$): 1.81 (4H, m), 2.69 (4H, m), 2.99 (3H, s), 3.02 (3H, s), 3.76 (2H, s), 7.35 (2H, d, J = 8 Hz), 7.43 (2H, m). HRMS (ES+) *m*/*z* 352.1620 ($[M+H]^+$ calcd for $C_{18}H_{21}F_3N_3O^+$ 352.1637).

1-{3-Fluoro-4-[2-oxo-2-(1-pyrrolidinyl)ethyl]phenyl}-3-(trifluoromethyl)-4,5,6,7-tetrahydro-1*H*-indazole (7i). Yield 10%. LCMS (ES+) *m*/*z* found 396, retention time 3.31 min. $C_{20}H_{21}F_4N_3O$ requires 395. ^{1}H NMR (400 MHz, $CDCl_3$): 1.80 (4H, m), 1.88 (2H, m), 1.98 (2H, m), 2.65 (2H, app br s), 2.72 (2H app br s), 3.50 (4H, m), 3.69 (2H, s), 7.24 (2H, m), 7.42 (1H, m). HRMS (ES+) *m*/*z* 396.1684 ($[M + H]^+$ calcd for $C_{20}H_{22}F_4N_3O^+$ 396.1699).

1-({4-[3-(Trifluoromethyl)-4,5,6,7-tetrahydro-1*H*-indazol-1-yl]-phenyl}methyl)-2-pyrrolidinone(7j). Yield 34%. LCMS (ES+) *m*/*z* found 364, retention time 3.18 min. $C_{19}H_{20}F_3N_3O$ requires 363. ^{1}H NMR (400 MHz, $CDCl_3$): 1.82 (4H, m), 2.02 (2H, m), 2.45 (2H, m), 2.69 (4H, m), 3.26 (2H, m), 4.50 (2H, m), 7.34 (2H, d, J = 8 Hz), 7.45 (2H, m).

1-({2-Fluoro-4-[3-(trifluoromethyl)-4,5,6,7-tetrahydro-1*H*-indazol-1-yl]phenyl}methyl)-2-pyrrolidinone (7l). Yield 15%. LCMS (ES+) *m*/*z* found 382, retention time 3.28 min. $C_{19}H_{19}F_4N_3O$ requires 381. ^{1}H NMR (400 MHz, $CDCl_3$): 1.82 (4H, m), 2.20 (2H, m), 2.43 (2H, m), 2.66 (2H, m), 2.72 (2H, m), 3.32 (2H, m), 4.54 (2H, s), 7.22−7.30 (2H, m), 7.50 (1H, t, J = 8 Hz).

1-{4-[(1,1-Dioxido-2-isothiazolidinyl)methyl]phenyl}-3-(trifluoromethyl)-4,5,6,7-tetrahydro-1*H*-indazole (7n). Yield 26%. LCMS (ES+) *m*/*z* found 400, retention time 3.31 min. $C_{18}H_{20}F_3N_3O_2S$ requires 399. ^{1}H NMR (400 MHz, $CDCl_3$): 1.83 (4H, m), 2.34 (2H, m), 2.69 (4H, m), 3.12 (2H, t, J = 6 Hz), 3.23 (2H, t, J = 8 Hz), 4.23 (2H, s), 7.47 (4H, m).

{4-[3-(Trifluoromethyl)-4,5,6,7-tetrahydro-1*H*-indazol-1-yl]-phenyl}methanol (7q). Yield 86%. LCMS (ES+) *m*/*z* found 297, retention time 3.06 min. $C_{15}H_{15}F_3N_2O$ requires 296. ^{1}H NMR (400 MHz, $CDCl_3$): 1.76 (1H, t, J = 6 Hz), 1.82 (4H, m), 2.69 (4H, m), 4.77 (2H, m), 7.48 (4H, m).

{4-[3-(Trifluoromethyl)-4,5,6,7-tetrahydro-1*H*-indazol-1-yl]-phenyl}acetonitrile (7r). Yield 60%. LCMS (ES+) *m*/*z* found 306, retention time 3.34 min. $C_{16}H_{14}F_3N_3$ requires 305. ^{1}H NMR (400 MHz, $CDCl_3$): 1.83 (4H, m), 2.70 (4H, m), 3.82 (2H, s), 7.44 (2H, d, J = 8 Hz), 7.53 (2H, m).

Preparation of 6-Substituted Bromo/Iodobenzene Reagents for Ullmann Couplings. 4-[(4-Iodophenyl)carbonyl]morpholine (6b). A solution of morpholine (653 mg, 7.5 mmol) in dichloromethane (40 mL) was cooled in an ice/methanol bath and then treated with stirring under argon with triethylamine (7.5 mmol, 1.05 mL) followed by the portionwise addition of 4-iodobenzoyl chloride (2.0 g, 7.5 mmol). The reaction mixture was allowed to stir at room temperature for 0.5 h before the solution was washed with water (2 × 20 mL). The organic layer was dried over sodium sulfate and evaporated under reduced pressure to give the title compound as a yellow solid (2.4 g, 100%). LCMS (ES+) *m*/*z* found 318, retention time 2.36 min. $C_{11}H_{12}INO_2$ requires 317. ^{1}H NMR (400 MHz, $CDCl_3$): 3.32−3.94 (8H, m), 7.15 (2H, m), 7.77 (2H, m).

1-[(4-Bromo-2-fluorophenyl)acetyl]pyrrolidine (6i). A mixture of (4-bromo-2-fluorophenyl)acetic acid (1.0 g, 4.29 mmol), pyrrolidine (305 mg, 4.30 mmol), and diisopropylethylamine (1.49 mL, 8.58 mmol) in dimethylformamide (15 mL) was stirred at room temperature under argon. Then HATU (1.79 g, 4.72 mmol) was added. The reaction mixture was allowed to stir at room temperature for 16 h. Dimethylformamide was removed by rotary evaporation, and the residual material was partitioned between ethyl acetate and water. The organic layer was separated and dried with sodium sulfate, and solvent was removed by rotary evaporation. The desired product was isolated by column chromatography on silica using 5−100% ethyl acetate in *n*-pentane to afford a white solid (0.97 g, 80%). LCMS (ES+) *m*/*z* found 286 and 288, retention time 2.61 min. $C_{12}H_{13}BrFNO$ requires 285 and 287. ^{1}H NMR (400 MHz, $CDCl_3$): 1.85 (2H, m), 1.96 (2H, m), 3.46 (4H, m), 3.60 (2H, s), 7.20−7.28 (3H, m).

1-[(4-Iodophenyl)methyl]-2-pyrrolidinone (6j). A solution of 2-pyrrolidinone (850 mg, 10 mmol) in dimethylformamide (40 mL) was cooled in an ice/methanol bath with stirring under an atmosphere of argon. Then a solid suspension of sodium hydride (60% in mineral oil, 440 mg, 11 mmol) was added portionwise over 10 min. The reaction mixture was allowed to stir with cooling for 30 min. Then 4-iodobenzyl bromide (2.97 g, 10 mmol) was added portionwise over 10 min. The whole mixture was allowed to warm slowly to room temperature and then stirred for a further 2 h. The reaction mixture was partitioned between ethyl acetate (100 mL) and water (200 mL). The organic layer was removed and reduced to minimum volume under reduced pressure. The residue was purified by column chromatography on a 20 g prepacked silica column, eluting from 0% to 100% ethyl acetate in petroleum ether to give the title compound as a yellow solid (2.97 g, 99%). LCMS (ES+) *m*/*z* found 302, retention time 2.59 min. $C_{11}H_{12}INO$ requires 301. ^{1}H NMR (400 MHz, $CDCl_3$): 2.01 (2H, m), 2.44 (2H, t, J = 8 Hz), 3.25 (2H, t, J = 7 Hz), 4.39 (2H, s), 7.00 (2H, d, J = 8 Hz), 7.66 (2H, m).

1-[(4-Bromo-2-fluorophenyl)methyl]-2-pyrrolidinone (6l). To a solution of 2-pyrrolidinone (0.62 g, 7.35 mmol) in DMF (20 mL) was added sodium hydride (60% suspension in mineral oil, 0.33 g, 8.2 mmol) portionwise under argon at room temperature, and the mixture was stirred for 15 min. Then 2-fluoro-4-bromobenzyl bromide (2.0 g, 7.46 mmol) was added. The resulting mixture was allowed to stir at room temperature for 5 h and allowed to stand at room temperature overnight. The reaction was quenched by the addition of water (2 mL). Then the mixture was evaporated under reduced pressure, partitioned between ethyl acetate and water, and dried with sodium sulfate. The solvent was removed by rotary evaporation to give an oil which was purified by column chromatography on silica using 10−100% ethyl acetate in *n*-pentane to give the title compound as colorless oil (1.70 g, 85%). LCMS (ES+) *m*/*z* found 272 and 274, retention time 2.52 min. $C_{11}H_{11}BrFNO$ requires 271 and 273. ^{1}H NMR (400 MHz, $CDCl_3$): 2.0 (2H, m), 2.43 (2H, m), 3.31 (2H, m), 4.46 (2H, s), 7.13−7.28 (3H, m).

2-[(4-Bromophenyl)methyl]isothiazolidine 1,1-Dioxide (6n). A solution of 4-bromobenzylamine (1.85 g, 10 mmol) and triethylamine (2 g, 20 mmol) in dimethylformamide (30 mL) was treated with 3-chloropropanesulfonyl chloride (1.78 g, 10 mmol) by dropwise addition over 10 min with stirring under argon. This mix was stirred for 30 min before being treated with a 60% suspension of sodium hydride in mineral oil (1.2 g, 30 mmol of NaH) portionwise and the whole mixture stirred at room temperature for 3 days. The reaction mixture was partitioned between water (50 mL) and dichloromethane (30 mL). The organic layer was dried over sodium sulfate and reduced to minimum volume by rotary evaporation. The residue was added to a 20 g prepacked silica column and eluted from 0% to 50% ethyl acetate in petroleum ether to give the title compound as a yellow oil (2.72 g, 94%). LCMS (ES+) *m*/*z* found 290, retention time 2.68 min. $C_{10}H_{12}{}^{79}BrNO_2S$ requires 289. ^{1}H NMR (400 MHz, $CDCl_3$): 2.32 (2H, m), 3.11 (2H, m), 3.21 (2H, m), 3.13 (2H, s), 7.24 (2H, m), 7.49 (2H, m).

1-[4-(1-Pyrrolidinylcarbonyl)phenyl]-3-(trifluoromethyl)-4,5,6,7-tetrahydro-1*H*-indazole (9a). A solution of 4-[3-(trifluoromethyl)-4,5,6,7-tetrahydro-1*H*-indazol-1-yl]benzoic acid (87 mg, 0.28 mmol) in dichloromethane (3 mL) was treated in one portion with solid 1,1′-carbonyldiimidazole (46 mg, 0.28 mmol). This mixture was allowed to stir at room temperature for 15 min. Pyrrolidine (23 mg, 0.32 mmol) was then added, and the stirring continued for 1 h at room temperature. The reaction mixture was then added to a 5 g prepacked silica column and eluted from 0% to 50% ethyl acetate in petroleum ether to give the title compound as a yellow oil (51 mg, 50%). LCMS (ES+) *m*/*z* found 364, retention time 3.22 min. $C_{19}H_{20}F_3N_3O$ requires 363. ^{1}H NMR (400 MHz, $CDCl_3$): 1.83 (4H, m), 1.91 (2H, m), 1.98 (2H, m), 2.70 (4H, m), 3.43 (2H, t, J = 6 Hz), 3.67 (2H, t, J = 6 Hz), 7.53 (2H, m), 7.64 (2H, m).

1-{4-[2-Oxo-2-(1-pyrrolidinyl)ethyl]phenyl}-3-(trifluoromethyl)-4,5,6,7-tetrahydro-1*H*-indazole (10a). A solution of {4-[3-(trifluoromethyl)-4,5,6,7-tetrahydro-1*H*-indazol-1-yl]phenyl}acetic acid (113 mg, 0.35 mmol) in dichloromethane (4 mL) in a Sarstedt tube was treated in one portion with solid 1,1′-carbonyldiimidazole (60 mg, 0.37 mmol). This mixture was shaken at room temperature for 30 min. Pyrrolidine (34 mg, 0.48 mmol) in dichloromethane (2 mL) was then added, and the shaking continued for 16 h at room temperature. The reaction mixture was washed with a mix of saturated sodium bicarbonate solution (4 mL) and brine (2 mL). The organic layer was then added to a 2 g SCX column and eluted with ethyl acetate (25 mL). The solvent was removed under reduced pressure and the residue purified by mass directed autoprep to give the title compound as a yellow oil (30 mg, 23%). LCMS (ES+) *m*/*z* found 378, retention time 3.28 min. $C_{20}H_{22}F_3N_3O$ requires 377. ^{1}H NMR (400 MHz, $CDCl_3$): 1.81 (4H, m), 1.88 (2H, m), 1.96 (2H, m), 2.69 (4H, m), 3.44 (2H, t, J = 7 Hz), 3.50 (2H, t, J = 7 Hz), 3.71 (2H, s), 7.38 (2H, d, J = 8

Hz), 7.43 (2H, m). HRMS (ES+) m/z 378.1775 ($[M + H]^+$ calcd for $C_{20}H_{23}F_3N_3O^+$ 378.1793).

({4-[3-(Trifluoromethyl)-4,5,6,7-tetrahydro-1*H*-indazol-1-yl]-phenyl}methyl)amine (14). Lithium aluminum hydride (12.4 mL, 2 M in THF solution, 24.9 mmol) and THF (30 mL) were stirred in an ice bath under argon. A solution of 4-[3-(trifluoromethyl)-4,5,6,7-tetrahydro-1*H*-indazol-1-yl]benzonitrile **7r** (1.81 g, 6.22 mmol) in THF (30 mL) was added dropwise over 15 min. Then the ice bath was removed and the reaction mixture was allowed to stir at room temperature for 1.5 h. Then the reaction mixture was cooled using an ice bath and quenched with water dropwise. Solvent was removed under reduced pressure. The residual material was diluted with dichloromethane and water. The insoluble solid was filtered off and the organic layer separated, washed with brine, and dried over sodium sulfate. The solvent was removed by rotary evaporation. The desired product was isolated using a 25 g SCX column initially washed with dichloromethane (30 mL), 1:1 dichloromethane/methanol (60 mL), and methanol (30 mL), and then the desired product was eluted with 1 M ammonia in MeOH (25 mL). The solvent was evaporated off under reduced pressure to give **20** as a brown oil (1.56 g, 85%). LCMS (ES+) m/z found 279 (M-16, ES+), retention time 2.16 min. $C_{15}H_{16}F_3N_3$ requires 295. ^{1}H NMR (400 MHz, $CDCl_3$): 1.82 (4H, m), 2.68 (4H, m), 3.93 (2H, s), 7.43 (4H, m).

***N*-({4-[3-(Trifluoromethyl)-4,5,6,7-tetrahydro-1*H*-indazol-1-yl]-phenyl}methyl)methanesulfonamide (15a).** A mixture of ({4-[3-(trifluoromethyl)-4,5,6,7-tetrahydro-1*H*-indazol-1-yl]phenyl}methyl)-amine **14** (1.56 g, 5.29 mmol) and triethylamine (1.48 mL, 10.58 mmol) in dichloromethane (40 mL) was stirred under argon in an ice bath. Methanesulfonyl chloride (1.21 g, 0.82 mL, 10.58 mmol) was added dropwise with stirring. The resulting mixture was allowed to stir at room temperature for 5 h. Then the reaction mixture was partitioned between dichloromethane and water. The organic layer was separated and dried over sodium sulfate. The desired product was isolated by column chromatography on silica using 10−70% ethyl acetate in *n*-pentane to give an oil which was then triturated with *n*-pentane to give **15a** as a white solid (1.60 g, 81%). LCMS (ES+) m/z found 374, retention time 3.12 min. $C_{16}H_{18}F_3N_3O_2S$ requires 373. ^{1}H NMR (400 MHz, $CDCl_3$): 1.82 (4H, m), 2.68 (4H, m), 2.92 (3H, s), 4.38 (2H, d, J = 6 Hz), 4.70 (1H, m), 7.43−7.54 (4H, m). HRMS (ES+) m/z 374.1138 ($[M + H]^+$ calcd for $C_{16}H_{19}F_3N_3O_2S^+$ 374.1150).

3-(Trifluoroacetyl)tetrahydro-4*H*-pyran-4-one (17). A solution of tetrahydro-4*H*-pyran-4-one **16** (5.0 g, 50 mmol) in tetrahydrofuran (100 mL) was cooled to −70 °C with stirring under argon. The solution was then treated with a 2 M solution of lithium diisopropylamide in tetrahydrofuran (25 mL) dropwise over 30 min. The mixture was then stirred at −70 °C for 30 min and then treated dropwise with ethyl trifluoroacetate (7.1 g, 5.9 mL, 50 mmol) with stirring under argon. The mixture was then allowed to warm slowly to 20 °C and stirred for 16 h under argon. The reaction mix was then partitioned between ethyl acetate (50 mL) and water (100 mL). The organic layer was dried over sodium sulfate and the solvent removed by rotary evaporation to give the title compound as a foamy yellow solid (10.34 g, 100%). LCMS (ES-) m/z found 195, retention time 2.35 min. $C_7H_7F_3O_3$ requires 196. ^{1}H NMR (400 MHz, CD_3OD) δ: 4.50 (2H, m), 3.87 (2H, m), 3.22 (1H, m), 2.34 (2H, m).

3-(Trifluoromethyl)-1,4,6,7-tetrahydropyrano[4,3-*c*]pyrazole (18). A mixture of 3-(trifluoroacetyl)tetrahydro-4*H*-pyran-4-one **17** (5.42 g, 27.7 mmol) and hydrazine hydrate (1.38 g, 1.4 mL, 27.6 mmol) in ethanol (120 mL) was stirred at 60 °C under argon for 6 h. A further 0.7 mL (14 mmol) of hydrazine hydrate was added, and the mixture was stirred at 70 °C for 3 h. The reaction mix was allowed to cool and the solvent removed by rotary evaporation. The residue was partitioned between dichloromethane and water. The organic layer was separated and dried over sodium sulfate, and solvent was removed by rotary evaporation. The aqueous layer was neutralized with 2 M HCl and re-extracted with dichloromethane. The organic layer was separated and dried over sodium sulfate, and the solvent was removed by rotary evaporation. The two organic extracts were combined to give the title compound as a yellow solid (3.64 g, 68%). LCMS (ES−) m/z found 191, retention time 1.92 min. $C_7H_7F_3N_2O$ requires 192; ^{1}H NMR (400 MHz, $CDCl_3$) δ: 11.32 (1H, br s), 4.76 (2H, s), 3.95 (2H, m), 2.83 (2H, m).

1-[(4-Iodophenyl)methyl]-2-pyrrolidinone (Precursor to 19b, 23b, and 28). A solution of 2-pyrrolidinone (3.15 g, 37.1 mmol) in dimethylformamide (130 mL) was cooled in an ice/methanol bath with stirring under an atmosphere of argon. Then a solid suspension of sodium hydride (60% in mineral oil, 1.48 g, 37.0 mmol) was added portionwise over 10 min. The reaction mix was allowed to stir with cooling for 30 min. Then 4-iodobenzyl bromide (10 g, 33.7 mmol) was added portionwise over 10 min. The whole mix was allowed to warm slowly to room temperature and then stirred for a further 3 h. The reaction mixture was partitioned between dichloromethane (150 mL) and water (100 mL). The aqueous layer was washed a second time with dichloromethane (100 mL). The combined organic layers were removed and washed with water (3 × 100 mL) and then brine (100 mL). The organic layer was dried over sodium sulfate and evaporated under reduced pressure to give the title compound as a yellow solid (9.98 g, 98%). LCMS (ES+) m/z found 302, retention time 2.57 min. $C_{11}H_{12}INO$ requires 301. ^{1}H NMR (400 MHz, $CDCl_3$) δ: 7.65 (2H, m), 7.00 (2H, m), 4.39 (2H, s), 3.25 (2H, m), 2.44 (2H, m), 2.00 (2H, m).

1-[4-(1-Pyrrolidinylcarbonyl)phenyl]-3-(trifluoromethyl)-1,4,6,7-tetrahydropyrano[4,3-*c*]pyrazole (19a). A mixture of 1-[(4-iodophenyl)carbonyl]pyrrolidine **18** (843 mg, 2.80 mmol), 3-(trifluoromethyl)-1,4,6,7-tetrahydropyrano[4,3-*c*]pyrazole **18** (563 mg, 2.93 mmol), copper(I) oxide (10 mol %, 0.3 mmol, 43 mg), *N*,*N*-dimethylglycine (20 mol %, 0.6 mmol, 62 mg), and cesium carbonate (5.8 mmol, 1.89 g) in dimethylsulfoxide (8 mL) was stirred at 130 °C for 16 h. The reaction mix was cooled and then partitioned between water (30 mL) and dichloromethane (2 × 20 mL). The organic layers were dried over sodium sulfate, and the solvent was removed under reduced pressure. The crude product was added to a 20 g isolute prepacked silica gel Sep-Pak column and eluted from 0% to 75% ethyl acetate in petroleum ether. The solvent was removed under reduced pressure to give the title compound as a yellow solid (616 mg, 60%). LCMS (ES+) m/z found 366, retention time 2.85 min. $C_{18}H_{18}F_3N_3O_2$ requires 365. ^{1}H NMR (400 MHz, $CDCl_3$) δ: 7.66 (2H, m), 7.58 (2H, m), 4.81 (2H, s), 3.94 (2H, t, J = 6 Hz), 3.67 (2H, t, J = 7 Hz), 3.44 (2H, t, J = 7 Hz), 2.90 (2H, t, J = 6 Hz), 2.03−1.88 (4H, m). HRMS (ES+) m/z 366.1418 ($[M + H]^+$ calcd for $C_{18}H_{19}F_3N_3O_2^+$ 366.1429).

1-({4-[3-(Trifluoromethyl)-6,7-dihydropyrano[4,3-*c*]pyrazol-1(4*H*)-yl]phenyl}methyl)-2-pyrrolidinone (19b). A mixture of 1-[(4-iodophenyl)methyl]-2-pyrrolidinone (150 mg, 0.5 mmol), 3-(trifluoromethyl)-1,4,6,7-tetrahydropyrano[4,3-*c*]pyrazole **18** (96 mg, 0.5 mmol), copper(I) iodide (10 mol %, 0.05 mmol, 10 mg), *N*,*N*-dimethylglycine (20 mol %, 0.1 mmol, 10 mg), and potassium carbonate (138 mg, 1 mmol) in dimethylsulfoxide (2 mL) was stirred at 190 °C in a microwave reactor for 30 min. The reaction mix was cooled and then partitioned between water (5 mL) and dichloromethane (5 mL). The organic layer was added to a 5 g isolute prepacked silica gel Sep-Pak column and washed through with ethyl acetate. The solvent was removed under reduced pressure and the residue purified via mass-directed autopreparation to give the title compound as a yellow oil (122 mg, 67%). LCMS (ES+) m/z found 366, retention time 2.72 min. $C_{18}H_{18}F_3N_3O_2$ requires 365. ^{1}H NMR (400 MHz, $CDCl_3$) δ: 7.48 (2H, m), 7.37 (2H, d, J = 8 Hz), 4.80 (2H, s), 4.51 (2H, s), 3.93 (2H, t, J = 6 Hz), 3.29 (2H, m), 2.87 (2H, t, J = 6 Hz), 2.46 (2H, m), 2.03 (2H, m). HRMS (ES+) m/z 366.1415 ($[M + H]^+$ calcd for $C_{18}H_{19}F_3N_3O_2^+$ 366.1429).

1-[(4-Bromo-2,6-difluorophenyl)methyl]-2-pyrrolidinone (Precursor to 19c). To a solution of 2-pyrrolidone (1.12 g, 13.23 mmol) in DMF (35 mL) was added sodium hydride (60% in

oil, 14.55 mmol, 0.58 g) portionwise under argon at room temperature, and the mixture was stirred for 15 min. Then 5-bromo-2-(bromomethyl)-1,3-difluorobenzene (3.78 g, 13.23 mmol) was added. The resulting mixture was allowed to stir at room temperature overnight. Then the reaction was quenched by the addition of water (2 mL). The DMF was evaporated off under reduced pressure and partitioned between ethyl acetate and water. The organic layer was washed with brine and dried over sodium sulfate. The solvent was removed by rotary evaporation to give an oil which was purified by column chromatography on silica using 10−100% ethyl acetate in *n*-pentane to give the title compound as an oil which then solidified on standing (3.18 g, 83%). LCMS (ES+) *m*/*z* found 290 and 292, retention time 2.56 min. $C_{11}H_{10}BrF_2NO$ requires 289 and 291. ^{1}H NMR (400 MHz, $CDCl_3$) δ: 7.10 (2H, m), 4.53 (2H, s), 3.27 (2H, m), 2.37 (2H, m), 1.97 (2H, m).

1-({2,6-Difluoro-4-[3-(trifluoromethyl)-6,7-dihydropyrano[4,3-*c*]pyrazol-1(4*H*)-yl]phenyl}methyl)-2-pyrrolidinone (19c). A mixture of 3-(trifluoromethyl)-1,4,6,7-tetrahydropyrano[4,3-*c*]-pyrazole **18** (0.99 g, 5.17 mmol), copper(I) oxide 0.74 g, 5.17 mmol), cesium carbonate (3.37 g, 10.34 mmol), 1-[(4-bromo-2,6-difluorophenyl)methyl]-2-pyrrolidinone (1.5 g, 5.17 mmol), and *N*,*N*-dimethylglycine (0.53 g, 5.17 mmol) in DMSO (15 mL) was heated at 130 °C under argon for 4 h. The reaction mixture was diluted with ethyl acetate. Catalyst was filtered off through Kieselguhr. The reaction mixture was partitioned between ethyl acetate and water, and the organic layer was separated, washed with brine, and dried over sodium sulfate. The solvent was removed by rotary evaporation, and the desired product was isolated by column chromatography on silica using 20−70% ethyl acetate in *n*-pentane. The residual material was recrystallized from ether to give the title compound as a white solid (0.62 g, 30%). LCMS (ES+) *m*/*z* found 402, retention time 2.90 min. $C_{18}H_{16}F_5N_3O_2$ requires 401. ^{1}H NMR (400 MHz, $CDCl_3$) δ: 7.18 (2H, m), 4.78 (2H, s), 4.60 (2H, s), 3.94 (2H, m), 3.30 (2H, m), 2.96 (2H, m), 2.40 (2H, m), 2.0 (2H, m). HRMS (ES+) *m*/*z* 402.1227 ($[M + H]^+$ calcd for $C_{18}H_{17}F_5N_3O_2^+$ 402.1241).

3-(Trifluoromethyl)-1,4,5,7-tetrahydropyrano[3,4-*c*]pyrazole (22). To a solution of (5,6-dihydro-2*H*-pyran-3-yloxy)(trimethyl)-silane[19] in dry THF (570 mL), a solution of methyllithium 1.6 M in diethyl ether (104 mL, 167 mmol) was added dropwise under argon at room temperature. After 2.5 h the mixture was cooled to −78 °C and then treated dropwise at this temperature with a solution of ethyl trifluoroacetate (23.7 g, 19.9 mL, 167 mmol) in dry THF (20 mL). The mixture was allowed to slowly warm to room temperature, stirred for 2 h, then quenched with saturated NH_4Cl solution (250 mL), keeping the internal temperature below 10 °C. The two layers were separated, and the aqueous layer was extracted twice with ethyl acetate (each with 250 mL). The resulting combined organic phase was finally dried over sodium sulfate and the solvent removed by rotary evaporation to give the intermediate 4-(trifluoroacetyl)dihydro-2*H*-pyran-3(4*H*)-one **21** as a foamy yellow solid (32.7 g, 100%).

21 (32.7 g, 167 mmol) was dissolved in ethanol (570 mL), and to the solution hydrazine hydrate (16.7 g, 16.6 mL, 334 mmol) was added at room temperature. The resulting mixture was stirred at reflux temperature for 6 h. Then it was allowed to cool to room temperature and the solvent was removed by rotary evaporation. The residue was partitioned between dichloromethane (400 mL) and water (200 mL). The aqueous layer was extracted twice with dichloromethane (each with 150 mL). The combined organic layers were washed with water (200 mL), brine (150 mL) and dried over sodium sulfate. The solvent was removed by rotary evaporation to obtain **22** as a yellow solid (20.5 g, 24%). LCMS (ES−) *m*/*z* found 191, retention time 0.58 min. $C_7H_7F_3N_2O$ requires 192. ^{1}H NMR (400 MHz, $CDCl_3$) δ: 13.28 (1H, br s), 4.68 (2H, s), 3.80 (2H, t), 2.61 (2H, m).

1-[4-(1-Pyrrolidinylcarbonyl)phenyl]-3-(trifluoromethyl)-1,4,5,7-tetrahydropyrano[3,4-*c*]pyrazole (23a). 23a was prepared from 1-[(4-iodophenyl)carbonyl]pyrrolidine and 3-(trifluoromethyl)-1,4,5,7-tetrahydropyrano[3,4-*c*]pyrazole **22** using method for **19a**: yield 25%. LCMS (ES+) *m*/*z* found 366, retention time 2.82 min. $C_{18}H_{18}F_3N_3O_2$ requires 365. ^{1}H NMR (400 MHz, $CDCl_3$) δ: 7.66 (2H, m), 7.49 (2H, m), 4.84 (2H, s), 3.97 (2H, t, J = 6 Hz), 3.67 (2H, t, J = 7 Hz), 3.44 (2H, t, J = 7 Hz), 2.84 (2H, t, J = 6 Hz), 2.02−1.88 (4H, m).

1-({4-[3-(Trifluoromethyl)-4,7-dihydropyrano[3,4-*c*]pyrazol-1(5*H*)-yl]phenyl}methyl)-2-pyrrolidinone (23b). 23b was prepared from 1-[(4-iodophenyl)methyl]-2-pyrrolidinone and 3-(trifluoromethyl)-1,4,5,7-tetrahydropyrano[3,4-*c*]pyrazole **22** using method for **19b**: yield 27%. LCMS (ES+) *m*/*z* found 366, retention time 2.76 min. $C_{18}H_{18}F_3N_3O_2$ requires 365. ^{1}H NMR (400 MHz, $CDCl_3$) δ: 7.38 (4H, m), 4.80 (2H, s), 4.50 (2H, s), 3.96 (2H, t, J = 6 Hz), 3.29 (2H, m), 2.83 (2H, m), 2.46 (2H, t, J = 8 Hz), 2.03 (2H, m). HRMS (ES+) *m*/*z* 366.1416 ($[M + H]^+$ calcd for $C_{18}H_{19}F_3N_3O_2^+$ 366.1429).

6-*tert*-Butoxycarbonyl-3-(trifluoromethyl)-4,5,6,7-tetrahydro-1*H*-pyrazolo[3,4-*c*]pyridine (26). A solution of lithium diisopropylamide in THF (40.2 mL, 2 M) was cooled to −78 °C with stirring under argon. To this was added a solution of 1-*tert*-butoxycarbonyl-3-piperidinone (16 g, 80.4 mmol) in THF (100 mL) with stirring under argon. The mixture was stirred at −78 °C for 20 min before being treated dropwise with ethyl trifluoroacetate (9.56 mL, 80.4 mmol). The reaction mixture was allowed to warm to room temperature and stirred for 2 h. The reaction mixture was quenched with water and neutralized with dilute aqueous hydrochloric acid. The reaction mixture was extracted with ethyl acetate. The organic layer was dried over sodium sulfate and evaporated under reduced pressure to give **25** as an orange foamy solid (23.6 g). LCMS (ES−) *m*/*z* found 294, retention time 3.31 min. $C_{12}H_{16}F_3NO_4$ requires 295. This material (23.6 g, 0.08 mol) in ethanol (250 mL) was treated with hydrazine monohydrate (4.16 mL, 0.086 mol). The mixture was allowed to stir at 50 °C for 24 h. The reaction mixture was cooled to room temperature and then evaporated under reduced pressure. The resulting mixture was partitioned between ethyl acetate and brine. The organic layer was separated and dried over sodium sulfate and evaporated under reduced pressure and the residual material recrystallized from ethyl acetate/*n*-pentane to give the title compound as a pale yellow solid (6.5 g, 28%). LCMS (ES−) *m*/*z* found 290, retention time 2.90 min. $C_{12}H_{16}F_3N_3O_2$ requires 291. ^{1}H NMR (400 MHz, $CDCl_3$) δ: 11.13 (1H, br s), 4.40 (2H, m), 3.66 (2H, m), 2.70 (2H, m), 1.48 (9H, s).

6-Methyl-3-(trifluoromethyl)-4,5,6,7-tetrahydro-1*H*-pyrazolo-[3,4-*c*]pyridine (27). Under an inert atmosphere of argon, $LiAlH_4$ (2.3 M in THF, 7.5 mL, 17.3 mmol) was added dropwise over 2 min to a cool (0 °C) stirring solution of 6-*tert*-butoxycarbonyl-3-(trifluoromethyl)-4,5,6,7-tetrahydro-1*H*-pyrazolo[3,4-*c*]pyridine **26** (2.00 g, 8.45 mmol) in anhydrous THF (42 mL). The resulting mixture was stirred in an oil bath at 58 °C for 17 h, cooled to 0 °C, and quenched by the careful addition of an aqueous solution of sodium potassium tartrate (1 M, 50 mL). After being stirred at room temperature for 1 h, the mixture was diluted with diethyl ether (50 mL) and more aqueous sodium potassium tartrate (1 M, 50 mL). After being stirred at this temperature for a further 1 h, the mixture was partitioned between water (100 mL) and diethyl ether (200 mL). The separated aqueous phase was extracted with ethyl acetate (200 mL), and the combined organic phase was dried ($MgSO_4$) and concentrated under vacuum. The resulting off-white solid (1.39 g) was purified using an SCX column giving the title compound as a yellow solid (1.23 g, 71%). LCMS (ES+) *m*/*z* found 206, retention time 2.90 min. $C_8H_{10}F_3N_3$ requires 205. ^{1}H NMR (400 MHz, $CDCl_3$) δ: 5.01 (1H, br s), 3.58 (2H, app s), 2.74 (4H, app s), 2.48 (3H, app s).

1-({4-[6-Methyl-3-(trifluoromethyl)-4,5,6,7-tetrahydro-1*H*-pyrazolo[3,4-*c*]pyridin-1-yl]phenyl}methyl)-2-pyrrolidinone (28). 28 was prepared from 1-[(4-iodophenyl)methyl]-2-pyrrolidinone and 6-methyl-3-(trifluoromethyl)-4,5,6,7-tetrahydro-1*H*-pyrazolo[3,4-*c*]-pyridine **27** from the method for **19a**: yield 40%. LCMS (ES+) *m*/*z*

found 379, retention time 1.72 min. $C_{19}H_{21}F_3N_4O$ requires 378. ^1H NMR (400 MHz, $CDCl_3$) δ: 7.41 (2H, m), 7.36 (2H, d, J = 9 Hz), 4.50 (2H, s), 3.58 (2H, s), 3.29 (2H, m), 2.81 (2H, m), 2.74 (2H, m), 2.50 (3H, s), 2.46 (2H, m), 2.03 (2H, m). HRMS (ES+) m/z 379.1735 ($[M + H]^+$ calcd for $C_{19}H_{22}F_3N_4O^+$ 379.1746).

Calcium Influx Fluorescence Assay. Stable recombinant GluA2 flip unedited cells were grown in DMEM/F12 and 10% FBS in a 5% CO_2 incubator in 175 cm^2 T-flasks 2−3 days before experiment cells were detached and seeded into 384-well black PDL-coated plates with clear bottom up to confluence. On the day of the experiment, cell plates were washed three times with assay buffer (mM: 20 HEPES, 145 NaCl, 5 KCl, 2 $CaCl_2$, 1 $MgCl_2$, 5.5 glucose, pH 7.3) and loaded with 2 μM Fluo4-AM for 60 min at room temperature. Cell plates were washed again to remove unloaded Fluo4 and placed into a FLIPR. A dual addition protocol was used to add compound solution 5 min before 100 μM glutamate stimulation. The glutamate-induced increased fluorescence was analyzed by using IDBS ActivityBase software and compared with positive control cyclothiazide.

Whole Cell Voltage-Clamp Electrophysiology Assay. This assay involved the electrophysiological characterization of AMPA receptor positive modulators using HEK293 cells stably expressing human GluA2 flip (unedited) subunits which form a functional homotetrameric AMPA receptor. The extracellular recording solution contained the following (in mM): 140 NaCl, 2 KCl, 1 $MgCl_2$, 2 $CaCl_2$, 12 *N*-[2-hydroxyethyl]piperazine-*N*-[2-ethanesulfonic acid (HEPES), 10 D-glucose, pH 7.35. The intracellular solution contained the following (in mM): 150 CsCl, 10 HEPES, 10 ethylene glycol bis(2-aminoethyl ether)-*N*,*N*,*N*′,*N*,-tetraacetic acid (EGTA), pH 7.3. For perforated patch recordings, intracellular solution containing amphotericin B (240 μg/mL) was used to backfill the pipet while intracellular solution alone was used to fill just the tip (the patch clamp pipettes have a resistance of between 2 and 5 MΩ). Amphotericin B creates small pores in the cell membrane beneath the electrode which allow small ions to pass across the membrane (and therefore allow electrical control of the cell) without the dialysis of second messenger molecules out of the cell, which could result in metabolic rundown of the cell leading to inconsistent receptor activation.[20] The membrane potential of the cell was held at −60 mV and perforated-patch clamp electrophysiology performed using EPC9 or -10 patch clamp system. Exchange of solution around the cell was achieved by using the RSC160 (Biologic) fast perfusion system to produce a rapid application of glutamate. Automatic series resistance and capacity compensation were applied and checked regularly. The current induced by a 2 s application of the agonist was recorded, and glutamate application was repeated every 30 s. Control currents elicited by a fixed concentration of agonist (1 mM glutamate) were recorded during the experiment in order to monitor any variations in charge. The compound was tested at two fixed concentrations (100 nM and 10 μM). As internal control during the experiments, a known AMPA receptor positive modulator was used. Response to 1 mM glutamate in the presence of compound was normalized against the response in the absence of compound that was considered 100%. Current analysis was performed after data acquisition and using zero subtraction function, measuring the net charge (time integration of the current) in the first 2000 ms from the onset of the peak and measuring the peak amplitude.

CLND Solubility Assay. For the kinetic solubility assay, 5 μL of 10 mM DMSO stock solution diluted to 100 μL with pH 7.4 phosphate buffered saline was used. The mixture was equilibrated for 1 h at room temperature and filtered through Millipore Multiscreen$_{HTS}$-PCF filter plates (MSSL BPC). The filtrate was quantified by suitably calibrated flow injection chemiluminescent nitrogen detection.[21]

Artificial Membrane Permeability Assay. The donor cell contained 2.5 μL of 10 mM sample solution in pH 7.05 phosphate buffer. To enhance solubility, 0.5% hydroxypropylcyclodextrin (Encapsin) was added to the buffer. The artificial membrane is prepared from 1.8% phosphatydilcholine and 1% cholesterol in decane solution. The sample concentration in both the donor and acceptor compartment is determined by LCMS after 3 h of incubation at room temperature.[22] The permeability (log P_{app}) measuring how fast molecules pass through the black lipid membrane is expressed in nm/s.

P450 CYPEX Assay. Inhibition (IC_{50}) of human CYPs 1A2, 2C9, 2C19, 2D6, and 3A4 was determined using Cypex Bactosomes expressing the major human P450s. A range of concentrations (0.1, 0.2, 0.4, 1, 2, 4, and 10 μM) of test compound were prepared in methanol and preincubated at 37 °C for 10 min in 50 mM potassium phosphate buffer (pH 7.4) containing recombinant human CYP450 microsomal protein (0.1 mg/mL; Cypex Limited, Dundee, U.K.) and probe-fluorescent substrate. The final concentration of solvent was between 3% and 4.5% of the final volume. Following preincubation, NADPH regenerating system (7.8 mg of glucose 6-phosphate, 1.7 mg of NADP, and 6 units of glucose 6-phosphate dehydrogenase/mL of 2% (w/v) $NaHCO_3$; 25 μL) was added to each well to start the reaction. Production of fluorescent metabolite was then measured over a 10 min time-course using a Spectrafluor Plus plate reader. The rate of metabolite production (AFU/min) was determined at each concentration of compound and converted to a percentage of the mean control rate using Magellan (Tecan software). The inhibition (IC_{50}) of each compound was determined from the slope of the plot using Grafit, version 5 (Erithacus Software, U.K.). Miconazole was added as a positive control to each plate. CYP450 isoform substrates used were ethoxyresorufin (ER, 1A2, 0.5 μM), 7-methoxy-4-triflouromethylcoumarin-3-acetic acid (FCA, 2C9, 50 μM), 3-butyryl-7-methoxycoumarin (BMC, 2C19, 10 μM), 4-methylaminomethyl-7-methoxycoumarin (MMC, 2D6, 10 μM), diethoxyflourescein (DEF, 3A4, 1 μM), and 7-benzyloxyquinoline (7-BQ, 3A4, 25 μM). The test was performed in three replicates.

Intrinsic Clearance (CLi) Assay. Intrinsic clearance (CLi) values were determined in rat and human liver microsomes. Test compounds (0.5 μM) were incubated at 37 °C for 30 min in 50 mM potassium phosphate buffer (pH 7.4) containing 0.5 mg of microsomal protein/mL. The reaction was started by addition of cofactor (NADPH, 8 mg/mL). The final concentration of solvent was 1% of the final volume. At 0, 3, 6, 9, 15, and 30 min, an aliquot (50 μL) was taken, quenched with acetonitrile containing an appropriate internal standard, and analyzed by HPLC−MS/MS. The intrinsic clearance (CLi) was determined from the first-order elimination constant by nonlinear regression using Grafit, version 5 (Erithacus Software, U.K.), corrected for the volume of the incubation and assuming 52.5 mg of microsomal protein/g of liver for all species. Values for CLi were expressed as (mL/min)/(g of liver). The lower limit of quantification of clearance was determined to be when < 15% of the compound had been metabolized by 30 min, and this corresponded to a CLi of 0.5 (mL/min)/(g of liver). The upper limit was 50 (mL/min)/(g of liver).

Acknowledgment. We thank Dr. Bill Leavens for HRMS data and Wai Chan for synthetic chemistry support.

Supporting Information Available: Cloning, expression, purification, crystallization, and crystallography of the rat GluA2 S1S2 ligand binding domain; statement on use of animals; analysis of blood, plasma, and brain samples from in vivo and protein binding studies; metabolite identification studies; high resolution mass spectometry methods; experimental procedures for molecules not described in manuscript. This material is available free of charge via the Internet at http://pubs.acs.org.

Note Added after ASAP Publication. This paper posted ASAP on December 3, 2010 with errors in Table 1, Figure 3 and Table 3. The corrected version was posted on January 6, 2011.

References

(1) Zarate, C. A., Jr.; Manji, H. K. The role of AMPA receptor modulation in the treatment of neuropsychiatric diseases. *Exp. Neurol.* **2008**, *211*, 7–10.

(2) Dingledine, R.; Borges, K.; Bowie, D.; Traynelis, S. F. The glutamate receptor ion channels. *Pharmacol. Rev.* **1999**, *51*, 7–61.

(3) Lynch, G.; Gall, C. M. Ampakines and the threefold path to cognitive enhancement. *Trends Neurosci.* **2006**, *29*, 554–562.

(4) Granger, R.; Staubli, U.; Davis, M.; Perez, Y.; Nilsson, L.; Rogers, G. A.; Lynch, G. A drug that facilitates glutamatergic transmission reduces exploratory activity and improves performance in a learning-dependent task. *Synapse* **1993**, *15*, 326–329.

(5) Ward, S. E.; Bax, B. D.; Harries, M. Challenges for and current status of research into positive modulators of AMPA receptors. *Br. J. Pharmacol.* **2010**, *160*, 181–190.

(6) Morrow, J. A.; Maclean, J. K.; Jamieson, C. Recent advances in positive allosteric modulators of the AMPA receptor. *Curr. Opin. Drug Discovery Dev.* **2006**, *9*, 571–579.

(7) Francotte, P.; de Tullio, P.; Fraikin, P.; Counerotte, S.; Goffin, E.; Pirotte, B. In search of novel AMPA potentiators. *Recent Pat. CNS Drug Discovery* **2006**, *1*, 239–246.

(8) Ward, S. E.; Harries, M.; Aldegheri, L.; Andreotti, D.; Ballantine, S.; Bax, B. D.; Harris, A. J.; Harker, A. J.; Lund, J.; Melarange, R.; Mingardi, A.; Mookherjee, C.; Mosley, J.; Neve, M.; Oliosi, B.; Profeta, R.; Smith, K. J.; Smith, P. W.; Spada, S.; Thewlis, K. M.; Yusaf, S. P. Discovery of *N*-[(2*S*)-5-(6-fluoro-3-pyridinyl)-2,3-dihydro-1*H*-inden-2-yl]-2-propanesulfonamide, a novel clinical AMPA receptor positive modulator. *J. Med. Chem.* **2010**, *53* (15), 5801–5812.

(9) Sobolevsky, A. I.; Rosconi, M. P.; Gouaux, E. X-ray structure, symmetry and mechanism of an AMPA-subtype glutamate receptor. *Nature* **2009**, *462*, 745–756.

(10) Jin, R.; Clark, S.; Weeks, A. M.; Dudman, J. T.; Gouaux, E.; Partin, K. M. Mechanism of positive allosteric modulators acting on AMPA receptors. *J. Neurosci.* **2005**, *25*, 9027–9036.

(11) Kaae, B. H.; Harpsoe, K.; Kastrup, J. S.; Sanz, A. C.; Pickering, D. S.; Metzler, B.; Clausen, R. P.; Gajhede, M.; Sauerberg, P.; Liljefors, T.; Madsen, U. Structural proof of a dimeric positive modulator bridging two identical AMPA receptor-binding sites. *Chem. Biol.* **2007**, *14*, 1294–1303.

(12) Sun, Y.; Olson, R.; Horning, M.; Armstrong, N.; Mayer, M.; Gouaux, E. Mechanism of glutamate receptor desensitization. *Nature* **2002**, *417*, 245–253.

(13) Differding, E.; Bersier, P. M. Electrochemical reduction of nitrogen-fluorine bonds: relevance to the reactivity of electrophilic fluorinating agents. *Tetrahedron* **1992**, *48*, 1595–1604.

(14) Hald, H.; Ahring, P. K.; Timmermann, D. B.; Liljefors, T.; Gajhede, M.; Kastrup, J. S. Distinct structural features of cyclothiazide are responsible for effects on peak current amplitude and desensitization kinetics at iGluR2. *J. Mol. Biol.* **2009**, *391*, 906–917.

(15) Ptak, C. P.; Ahmed, A. H.; Oswald, R. E. Probing the allosteric modulator binding site of GluR2 with thiazide derivatives. *Biochemistry* **2009**, *48*, 8594–8602.

(16) Dunitz, J. D.; Taylor, R. Organic fluorine hardly ever accepts hydrogen bonds. *Chem.—Eur. J.* **1997**, *3*, 89–98.

(17) Foley, A. G.; Murphy, K. J.; Hirst, W. D.; Gallagher, H. C.; Hagan, J. J.; Upton, N.; Walsh, F. S.; Regan, C. M. The 5-HT(6) receptor antagonist SB-271046 reverses scopolamine-disrupted consolidation of a passive avoidance task and ameliorates spatial task deficits in aged rats. *Neuropsychopharmacology* **2004**, *29*, 93–100.

(18) Ennaceur, A.; Delacour, J. A new one-trial test for neurobiological studies of memory in rats. 1: Behavioral data. *Behav. Brain Res.* **1988**, *31*, 47–59.

(19) Eiden, F.; Wanner, K. T. Pyrans, 100. 5,6-Dihydro-2*H*-pyran-3(4*H*)-one as a synthon for pyran-annulated heterocyclic compounds. *Liebigs Ann. Chem.* **1984**, 1759–1777.

(20) Virginio, C.; Giacometti, A.; Aldegheri, L.; Rimland, J. M.; Terstappen, G. C. Pharmacological properties of rat alpha 7 nicotinic receptors expressed in native and recombinant cell systems. *Eur. J. Pharmacol.* **2002**, *445*, 153–161.

(21) Bhattachar, S. N.; Wesley, J. A.; Seadeek, C. Evaluation of the chemiluminescent nitrogen detector for solubility determinations to support drug discovery. *J. Pharm. Biomed. Anal.* **2006**, *41*, 152–157.

(22) Veber, D. F.; Johnson, S. R.; Cheng, H. Y.; Smith, B. R.; Ward, K. W.; Kopple, K. D. Molecular properties that influence the oral bioavailability of drug candidates. *J. Med. Chem.* **2002**, *45*, 2615–2623.